PORE NETWORK MODELING OF GAS TRANSPORT

IN SOURCE ROCKS

A Dissertation

by

SAAD FAHAID K. ALAFNAN

Submitted to the Office of Graduate and Professional Studies of
Texas A&M University
in partial fulfillment of the requirements for the degree of

DOCTOR OF PHILOSOPHY

Chair of Committee,	Ibrahim Yucel Akkutlu
Committee Members,	Yalchin Efendiev
	John Killough
	Eduardo Gildin
Head of Department,	Daniel Hill

December 2017

Major Subject: Petroleum Engineering

ABSTRACT

Source rocks such as resource shale are a special subclass of petroleum reservoirs where the hydrocarbons are generated and stored in the same place. They consist of diverse minerology including clays, silt, quartz, carbonates as well as varying amount of organic material. This diversity creates a multi-scale pore network including pores down to a few nanometers, micro-cracks and fractures, which influences the fluid storage and transport in the formation. In this dissertation, initially I present an upscaling study to gas transport in nano-scale within the organic material of the source rock via pore network modeling approach. The nanoscale transport effects are linked to the reservoir scale honoring the multi-physics and multi-scale nature of the formation. The pore network model is built in accordance with three-dimensional nano-scale imaging of shale samples where, in most of the cases, the organic material is observed as a network of pores with some micro-cracks of larger size cutting through, or by the edge of, the material.

The interaction between the networks of organic pores and micro-cracks could be important for natural gas production from source rock, because it can control the rates at which the fluid is transported from the organic constituents of the formation. The matrix-fracture interactions could also be influenced by the existing in-situ stresses. Understanding the transient flow behavior would eventually help us optimize production.

At high pressure, gas is stored in the organic material as a compressed free gas and adsorbed gas. Its transport is driven by pressure gradient with some additional fluxes caused by the degree of confinement and the presence of an adsorbed layer which can be mobile under some conditions of high pressure gradient. A modified pressure dependent definition of a scaled up organic material permeability is obtained taking into account the previously mentioned factors and using the concept of percolation theory. This permeability can be used with the classical governing equations of flow and transport. The coupling term relating the fluid exchange between the organic material and the associated micro-cracks and fractures is derived and validated through the concept of dual porosity relating the total fluid exchange to the pressure difference at the fracture-matrix interface with some modifications to account for the captured transient effect and the pressure dependency of the gas properties.

At the final part of the thesis, I present a reservoir grid-block scale application of the derived organic nanoporous matrix-fracture coupling by implementing the formulation into conventional diffusivity formulation. The results show the retardation effect on production due to presence of organic nanopores. In addition, the role the transport mechanisms in the organic material play on the production is analyzed.

ACKNOWLEDGEMENTS

I would like to thank my committee chair, Professor Yucel Akkutlu, and my committee members Professor Yalchin Efendiev, Professor John Killough, and Professor Eduardo Gildin for their guidance and support throughout the course of this research.

Thanks also go to my friends and colleagues and the department faculty and staff for making my time at Texas A&M University a great experience. I also want to extend my gratitude to King Fahad University of Petroleum and Minerals, the Saudi Culture Mission in the USA, and Saudi Aramco, which sponsored me as a PhD student.

Finally, thanks to my mother and father for their encouragement and to my wife for her love and patience.

CONTRIBUTORS AND FUNDING SOURCES

Contributors

This work was supervised by a dissertation committee consisting of Professor Yucel Akkutlu (chair advisor) and Professor Yalchin Efendiev of the Mathematics Department and Professor Eduardo Gildin of the Department of Petroleum Engineering and Professor John Killough of the Department of Petroleum Engineering.

All work for this dissertation was completed independently by the student.

Funding Sources

Graduate study was supported by a sponsorship from King Fahad University of Petroleum and Minerals, Saudi Culture Mission in USA, and Saudi Aramco.

TABLE OF CONTENTS

LIST OF FIGURES

Page

LIST OF TABLES

Page

1. INTRODUCTION

Resource shales are a subclass of petroleum reservoirs where the rock itself serves as both the source, from which the petroleum is generated, and the place, where it is stored. The production from shales was economically unfeasible and technically difficult until the recent breakthrough in horizontal drilling and hydraulic fracturing.

Shales mainly consist of inorganic minerals such as clays, silt, quartz, carbonates, feldspars and organic materials such as kerogen, which yields the fluid hydrocarbons, and bitumen. Shales are special class of porous media because of multi-scale and multi-physics nature of the fluid hydrocarbons storage and transport. Natural gas, for example, is stored in a compressed form in the pores that belong to the inorganic portion of the matrix; in addition, it can be found as sorbed (adsorbed + absorbed) fluid in the pores that belong to the organic constituents of the shale.

The flow in porous media equations are built based on two main petrophysical parameters: porosity, as a measure of the fluid storage capacity of the formation, and permeability, as the measure of the transport and production rates. These quantities are average measures of the porous medium that allow continuum description of fluid storage and transport. The multi-scale and the multi-physics nature of the shale formation make direct application of the conventional unipore description of fluids in porous media and the related principles of transport insufficient.

Organic materials have chemical composition similar to the hydrocarbon fluid stored therein. The storage and transport develops in the organic material mainly within

pores with sizes in the order of 1-10 nanometers. These pore have characteristically large specific surface area for the adsorption of the hydrocarbon fluids. The rapid desorption of the adsorbed fluid molecules is controlled by mainly the pore pressure. Hence, these factors related to storage and transport within the organic matter must be taken into consideration when describing the hydrocarbon fluid transported in shale.

In general, there is a lack of well-established understanding of the different transport mechanisms in the organic material and their relative importance. Additionally, the interactions and coupling between the organic nanopore network and the other constituents of the shale matrix pore structure are not well-understood at reservoir scale. Much work has been done modeling the transport of gas in organic materials assuming single capillary model, which served as the basis to understand the physics of the transport mechanisms that exist in the organic material. However, these equations are difficult to implement directly because in reservoir engineering, macroscopic equations are used based on the concept of representative elementary volume of fluid saturated porous medium, rather than performing the calculations capillary by capillary which is computationally unfeasible. Hence, it is of our interest to obtain a macroscopic approach that honors the physics that are observed at the microscopic level.

Various upscaling methods can be followed for the purpose. However, since most of the recent research on transport in the organic material is given in the literature in a single capillary form, the pore network modeling and simulation would be a natural upscaling approach because the pore network modeling considers the single capillary as a throat connecting the nodes, or pores, of the network and, hence, the equation

describing transport in a single capillary can be used directly to interconnect the pore network hydraulically.

In this dissertation, a multi-scale pore network modeling approach will be used to study the transport within the organic matter in shales. More specifically, the organic nanopore network will be designed to discharge to a fracture with a length in the order of a micron.

1.1 Literature Review*

While the production techniques from the source rocks such as the shale formations have advanced noticeably to make these formations one of the major energy resources in recent years, the uncertainties associated with the shale petrophysics limit the ability to fully manage and optimize shales wells. Shale formation has a multi-scale pore structure with a nano-scale degree of confinement associated with its organic constituent known as kerogen. Moreover, the transport in the organic material is complex and deviates from the well-known Darcy's law, which makes the direct applications of the conventional concepts of fluid transport in porous media imprecise. In shales, natural gas can be stored as compressed fluid, also known as free fluid, in the organic and inorganic pores. In addition, gas accumulates on the large surfaces of the organic nanopores as adsorbed fluid. When the shale matrix is subject to pressure

* Reprinted with permission from "Matrix-Fracture Interactions during Flow in Organic Nanoporous Materials under Loading" by Saad Alafnan & Yucel Akkutlu, 2017. Journal of Transport in Porous Media.

gradient, the free gas is transported first. Then, the adsorption equilibrium is shifted favoring the rate of molecular desorption. Hence, the transport in shale exhibits advective-diffusive-adsorptive in the organic nanopores, in addition to advection in the inorganic matrix.

The complexity of the transport is not just limited to its multi-scale and multi-physics nature but also to the different responses of organic and inorganic pores under confining stresses due to their geometrical shapes (Hsieh et al., 2015). The organic pores which have round shapes tend to distribute the stresses without significant deformation unlike the inorganic slit-like pores. The aforementioned complications make the transport in shales an active area of research.

Klinkenberg (1941) noticed the deviation of the permeability of a porous medium from Darcy's law and proposed an empirical factor as the correction. The deviation is caused by slipping gas molecules near the pore walls and can be a major factor in the case of tight source rock formations with a significant number of nanopores. Knudsen diffusion could be relative importance when compared to the viscous effect at a large degree of nano-scale confinement. Ertekin (1986) presented a modified version of Darcy's law including Knudsen diffusion. Javadpour (2009) incorporated advection with slip-flow and Knudsen diffusion to obtain an apparent permeability for straight nano-capillaries. Singh et al. (2014) followed similar approach but for tortuous slit and cylindrical pores. Furthermore, he proposed an effective permeability model based on the statistical sum of the two types of pores assuming an idealized log-normal distributions of both of them. In summary, these models dealt with the advective-

diffusive flow regimes of shales either empirically or analytically but the role of the adsorbed phase was not incorporated in their works.

On the other hand, some other models such as Sakhaee-Pour and Bryant. (2012); Akkutlu and Fathi (2012); Wasaki and Akkutlu (2015) included the adsorbed phase in their approaches. Sakhaee-Pour et al. (2012) considered the adsorbed phase as immobile and proposed an apparent permeability formulation of nanopores corrected for the pore space taken by the adsorbed layer while, Akkutlu and Fathi (2012) accounted for the co-existence of Knudsen diffusion and surface diffusion in the organic constituents of shales. Wasaki and Akkutlu (2015) followed a similar approach but considering additionally that the inorganic matrix is stress-sensitive. The sensitivity is considered the most influential on the micro-crack permeability, which was modeled using an equation developed by Gangi (1978).

In general, all the aforementioned studies have point out different aspects of natural gas transport in shales. They all signify the role of diffusive mechanisms in nanopores, such as Knudsen diffusion and surface diffusion, as the means of transport. However, the role of those organic nanopores on the fluid dynamics in a bigger picture of a more complex shale matrix has not been addressed comprehensively yet. It is thus my interest in this thesis to study the advective-diffusive-adsorptive transport in the organic pore network and then, couple the network to the larger features of the shale matrix pore structure to study their multi-scale interactions during the production. The concept of pore network modeling can be used for that purpose where capillaries of different properties representing the organic and inorganic components of shale matrix

can be interconnected and monitored closely. The results can then be used to derive a scaled-up model that interprets all the aspects of the shale transport into some useful reservoir engineering quantities for the field scale applications.

When looking at the two-dimensional scanning electron microscopy (SEM) images of shales, the finely-dispersed organic pockets can be seen within the inorganic matrix. In these images the organic material is often associated with cracks, which either cuts through the organic pocket or develops right by their edges at the boundaries of the organic and inorganic materials as shown in Figure 1. These cracks are a side-effect of the organic matter maturation in brittle source rocks. It is well-documented in the literature that these cracks are stress-sensitive such that their ability to transmit the stored fluids can be significantly reduced, when they are exposed to external load such as overburden stress, using crack models (Sneddon and Elliot, 1946; Mavko and Nur, 1978; Gangi, 1978) and based on the laboratory experiments with shale samples (Kwon et al., 2004; Akkutlu and Fathi, 2012; Heller and Zoback, 2013). However, mechanical interaction of the cracks with the surrounding nanoporous organic matrix needs to be investigated. This is an important task because, the stress-sensitive cracks are part of a multi-scale pore network of pores and fractures that feeds into the wellbore and, during the production of natural gas, the nature of interaction could potentially impact the production rates and reserve. In essence, the cracks serve as the conduit of shale fluids from the organic to the inorganic matrices and, finally, to the hydraulic fracture.

Despite their nano-scale size, the organic material may contribute significantly to the overall storage of hydrocarbon fluids due to their relatively large surface area

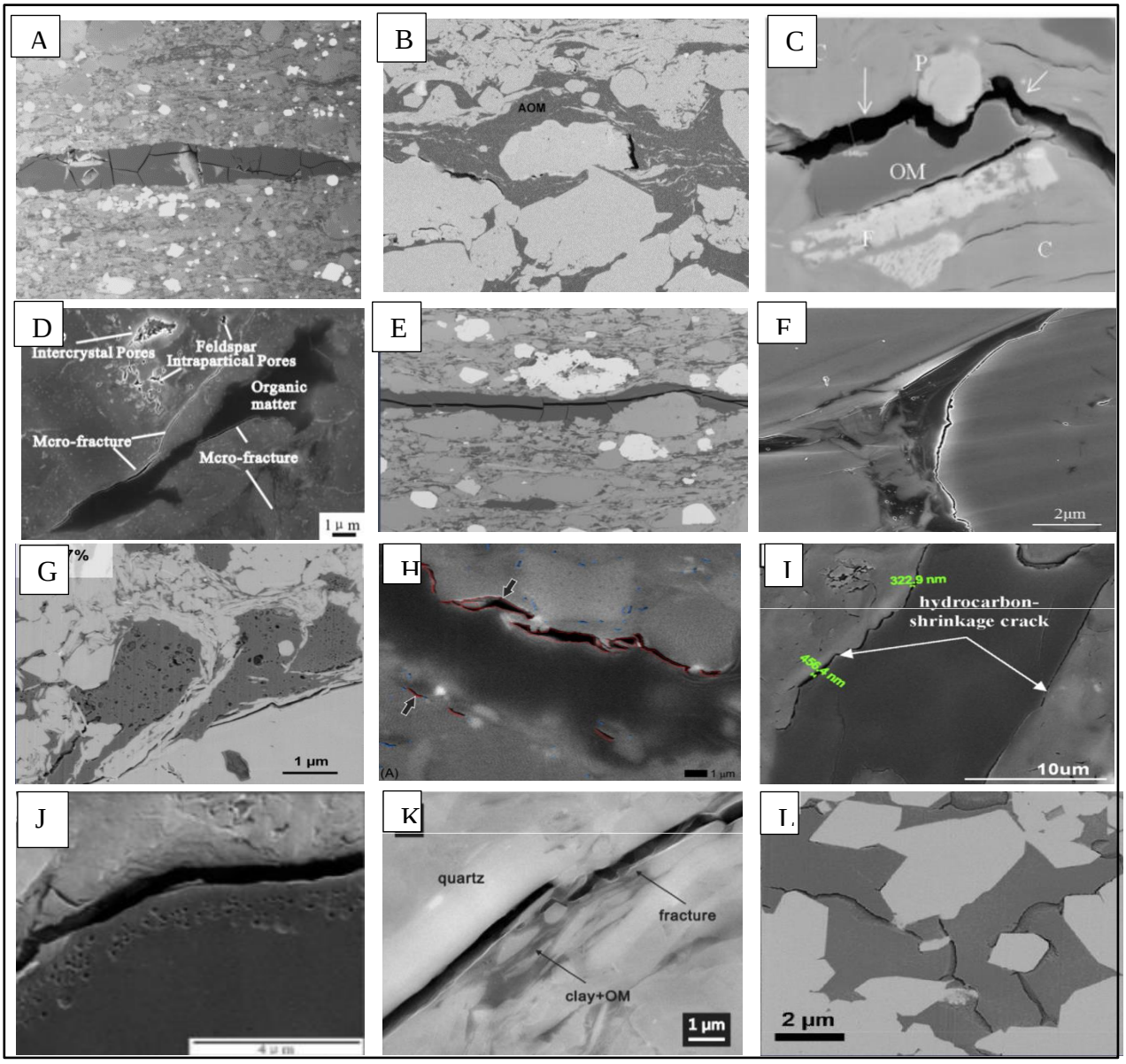

Figure 1 – Different SEM images showing organic material in darker color and cracks in black either by the edge of the organic material or cutting through it. A from Curtis (2013); B from Cardott et al. (2015); C from Zhang (2017); D from Hou et al. (2015); E from Curtis (2013); F from Zhou et al. (2016); G from Curtis (2013); H from Klaver et al. (2016); I from Yang et al. (2016); J from Chen et al. (2016); K from Jiao et al. (2014); L from Curtis (2013).

(Ambrose et al., 2012). The transport mechanisms in these nanopores are of non-Darcian nature (i.e. deviates from Stoke's flow) and can be modeled by considering the nano-scale wall-induced effects discussed in Kang et al. (2011), Fathi and Akkutlu (2012), Rahmanian et al. (2013), and Javadpour et al. (2013). Linking the local storage and transport properties in organic nano-capillaries to a crack for a better understanding of the matrix-fracture duality and investigating the coupling between them is the objective of my study.

In this thesis, I will start with description of the flow in single organic nano-pore, or capillary, and follow a step by step upscaling approach using the pore network modeling to describe the dynamics of the natural gas transport in the organic matrix. Kou et al. (2016) proposed an equation for the single organic nano-capillary that accounts for the advective-diffusive-adsorptive nature of the transport based on the results obtained from molecular dynamics simulation of methane molecules. Their approach will be used as the governing equation of gas flow in the organic nanopores while the classical Stoke's equation will be used for the flow in the crack.

1.1.1 Pore Network Modeling

Since it was first introduced by Fatt in 1956, pore network modeling approach to simulate flow in porous medium has widely been used in petroleum reservoir engineering, chemical engineering, environmental engineering and nuclear safety (Blunt 2001). The idea of network modeling can be very helpful in relating the microscopic coefficients to some meaningful macroscopic transport parameters. In petroleum

engineering, the pore network modeling has been used to investigate important flow parameters such as the absolute permeability, the fluid saturation-dependent relative permeability, and capillary pressure. Network modeling is an approach where capillaries (or throats) of random radii are interconnected at pore bodies (or nodes) distributed in three dimensions to form a lattice that represents the porous medium. Various ways capillaries connecting the neighboring pores make up the coordination number of the medium, which reflects the pore-network connectivity and, hence, control tortuosity, local permeability heterogeneity and anisotropy of the pore network. Traditionally the Hagen-Poiseuille equation is used to describe laminar flow in a single capillary. By performing a mass balance around each pore for all of the pores, a system of linear algebraic equations can be obtained and numerically solved for the pore pressure and flow rate. Subsequently, the desired macroscopic parameters of the system can be obtained.

The pore network modeling consists of two main building blocks: pores and throats. The former serve as the locations of fluid storage and are interconnected using throats which serve as the fluid transport paths (Celia et al., 1992). The size of the throats determines how permeable the system is while the size of the pores and the compressibility of the fluids determines the storage capacity of the system under certain conditions. Depending on the nature of the pore structure and the phenomena being studied, the size and the shape of the pores and throats can be selected (Joekar-Niasar et al., 2012).

Much work has been done on the hydrocarbon fluids transport in a single capillary in order to understand the transport in shales. Models are usually similar to that derived from Stokes flow equations but with some additional factors to account for the additional flux induced by the walls of the nano-capillary. Using network model approach would enable linking the microscopic effects to a macroscopic form that is useful for upscaled reservoir flow simulation. Some effort has been previously done in the upscaling of these single capillary equations. In some cases a bundle of capillaries approach is used (Kuila et al., 2013; Riewchotisakul and Akkutlu, 2015). The limitation of this approach is that the bundle does not reflect the complexity of the porous medium where pores could be interconnected to form a complex network of flow pathways rather than straight flow streams. Mehmani et al. (2013) presented a study where nanopores are introduced to a network of interconnected nanocapillaries and showed that the overall transport of the fluid can be dictated by those nanopores that make up 20% of the total pores. That would have not been the case, if a bundle of capillaries approach had been used, when the smaller capillaries would not have a significant impact on the transport within the shales.

1.1.2 Single Capillary Equation

Flow equation in a single throat is the backbone of the pore network model. The well-known Hagen-Poiseuille (HP) equation for viscous flow in a capillary is traditionally used:

$$q_{HP} = \frac{\pi R^4}{8\mu}\frac{dP}{dL} \qquad (1)$$

HP flow equation is insufficient to describe the fluid flow in small nano-capillaries. At nano-scale, the organic capillary wall effects on the flow might be significant especially at small capillary sizes. A modified version of the HP equation is discussed in several publications to account for diffusive flow regime. The form of the flow equation depends on the physical and chemical phenomena that involve multi-component non-Newtonian fluid. It is also dependent on the chemical and physical interactions between the fluids and the organic nano-capillary walls. In the case of shale gas flow in nano-capillaries, the adsorbed phase comes into play in unique ways. Firstly, if the capillary is exposed to large pressure drop, the transport experiences the contribution of the desorbed gas molecules. In addition, in general, it has been shown that the adsorbed hydrocarbon molecules such as methane, can be mobile and contribute significantly to the overall transport. Kou et al. (2016) recently argued that the adsorbed methane transport can be modeled as cluster diffusion and proposed a modified version of the HP equation to account for the adsorptive-diffusive transport of natural gas in the organic nano-capillary.

$$q_{tube} = \frac{\pi R_a^4}{8\mu}\frac{dP}{dL} + \frac{D_k}{P}\pi R_a^2\frac{dP}{dL} + \frac{\rho_{ads}}{\rho_{bulk}}D_s\pi(R_{tube}^2 - R_a^2)\frac{dP}{dL} \quad (2)$$

Here, R_{tube} and R_{ads} are the capillary radius and the corrected radius for the presence of an adsorption layer, respectively. D_K is the Knudsen diffusivity coefficient of the natural gas. D_s is the adsorbed phase mobility obtained from molecular dynamics simulations (*i.e.*, $V_{ads} = D_s\, dP/dL$). This form is selected because, in addition to the viscous diffusive mechanisms, the overall transport in the capillary also experiences the cluster diffusion

which can contribute to the transport under a certain range of pressure and degree of confinement (Riewchotisakul and Akkutlu, 2016; Kou et al., 2016).

The terms that appear on the right hand side of equation (2) are dependent on the average pressure across the capillary. Density of the adsorbed phase can be obtained empirically using the molecular simulation of gas in nanotubes (Riewchotisakul and Akkutlu, 2015) and the density of the bulk phase is calculated using the real gas law. D_k is the Knudsen diffusivity of gas and it is dependent on the gas properties, pore diameter, and the temperature. It can be obtained analytically from the kinetic theory of gases (Cunningham et al., 1980).

$$D_k = \frac{d_p}{3}\sqrt{\frac{8\,R\,T}{\pi\,M}} \qquad (3)$$

where, d_p is the diameter of capillary, M is the molecular weight, T is the temperature and R is the universal gas constant.

1.2 Scope of Work

The main objective of this dissertation is to understand the transport within the organic rich source rocks such as the shale formation by looking beyond the hydraulic fractures deep into the formation, into one of its major constituents which is the nanoporous organic material and the associated cracks. The goal is to obtain an upscaled model of the transport within the nanoporous organic material starting from a single nano-capillary equation that is given by Kou et al. (2016). The microscopic equation needs to be taken to a macroscopic representative elementary volume level via pore

network modeling approach. I would also study the relative importance of each transport mechanism within the organic material and the conditions at which one or more of these mechanisms prevail in the organic pore network. Additionally, the influence of organic material on the dynamics of the cracks under reservoir conditions is to be investigated using a multi-scale pore network model that is built in accordance with the scanning electron microscopy images in order to derive a expression to describe the organic material-crack coupling. This coupling term can be time-dependent and will be used along with the classical mass balance equations at the reservoir simulation block scale in order to predict the exchange rate of fluid between the two media during both the transient and the pseudo-steady state flow regimes using an approach similar to the one given by (Zimmerman et al., 1993) with some modifications to account for the multi-scale and multi-physics nature of the transport in the shale matrix.

1.3 Dissertation Outline

In this research, we present a study on the transport of natural gas from the organic materials into the cracks starting from a single capillary equation to a macroscopic scale via pore network modeling.

In section 2, the apparent permeability of the organic material is investigated under various conditions of pore pressure, pressure gradient, applied stresses, and size distributions of pores and throats. The results are linked with the percolation theory to obtain an apparent permeability model that has some coefficients accounting for the viscous, diffusive, and adsorptive transport mechanisms within the organic materials.

In section 3, the pore network model concept is extended by implementing some micro-cracks within the organic materials in a multi-scale and multi-physics representation of shale. Next, a dual porosity approach is used to describe the gas flow exchange between organic pores and cracks.

In section 4, the coupling term derived for the fluid exchange between the organic material and the cracks is used in a reservoir simulation grid block scale to assess the role of organic material on the overall natural gas production from a shale gas well.

2. GAS TRANSPORT IN THE ORGANIC MATERIALS

2.1 Pore Network Modeling

Scanning electron microscopy images of the organic constituent of shale samples clearly showed that the pores and the throats take a round shape (Wang and Reed 2009; Ambrose et al. 2010; Ambrose et al. 2012; Singh et al. 2014). I decided to build a pore network model that is consistent with this observation. The organic pores in my pore network model have spherical shape and they are interconnected with throats of cylindrical shape.

The pore and throat sizes indeed vary in the organic material. Different techniques can be used to measure this variation such as mercury injection test where, using a piston, liquid mercury is forced to penetrate the capillaries in the sample. The higher the force is applied, the smoller capillaries mercury penetrates. The result is a pore size distribution of the sample. In my work, I used such a distribution with a mean and variance to reflect the variability in the sizes of pores and throats that are interconnected, see in Figure 2.

Equation 4 is written at each node (pore) where the first term represents the sum of all fluxes coming and leaving the node, and the second term represents the net accumulation of gas in the node.

$$\sum_{1}^{n} \rho_{gi} q_i + \frac{d(\rho_g V_P)}{dt} = 0, \tag{4}$$

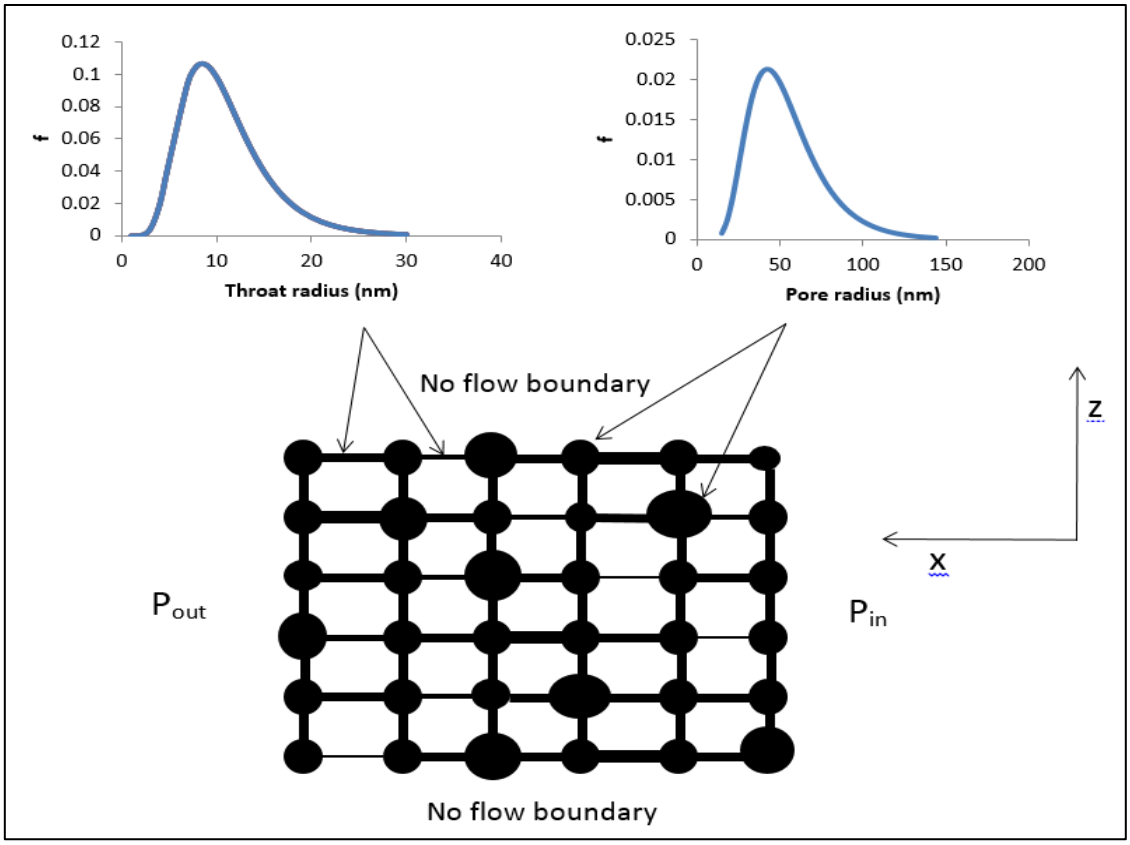

Figure 2 — Two-dimensional schematic of the three-dimensional organic nanopore-network construction using pore and throat size distributions.

The flow rate in the first term is given by equation 2 which accounts for the additional diffusive-adsorptive terms. *n* is the coordination number which is the number of capillaries interconnected at a given pore. The pore volume in the second term is subject to expansion and shrinkage depending on the assigned value of the pore compressibility, c_r. The discretization of equation 4 gives an algebraic equation with pressure dependent coefficients which is solved iteratively using Newton Raphson method.

My nanopore network model allows interconnecting pores up to 22 directions with their neighbors to fully capture the heterogeneity and anisotropy of the pore network system. The chosen coordination number would dictate the level of communication among the pores and the direction of heterogeneity in the network. In the case of real samples, micro-CT scanning and SEM along with the size distributions are transformed into pore network model for fluid dynamic analysis (Bultreys et al., 2016). In my case and because the main purpose of this work is to study the transport within organic materials in general, I have created my pore network model randomly based on a reasonable selection of coordination number, and size distributions of throats and pores that are in agreement with what is available in the literature (O'Carroll et al. 1993). The pore network model is a cube with its size being determined by the number of pores and length of the throats connecting them in the x, y, and z directions. Typically the size of my network is about 1 micron^3. No flow boundary condition is implemented at the outer boundaries of the cube except for the inlet and outlet pressures, which are assigned along the x-direction to create a pressure gradient as shown in Figure 2.

2.2 Representative Elementary Volume (REV)

One of the goals of my work is to obtain the smallest REV of the organic nanopore network over which the measured macroscopic quantities such as porosity and permeability would yield a meaningful average value that is representative of the whole system. Below REV these quantities are meaningless since they fluctuate significantly.

Using the pore network model described previously, permeability of the network is obtained as a function of the lattice volume. For this purpose I developed pore network models with varying sizes for the gas flow and transport experiment. In each experiment I allowed sufficient time for the steady-state gas flow to be established across the pore network and applied Darcy's law to estimate the systems permeability. This can be done relatively easily since under steady-state the flow rate (or fluid flow velocity) of the natural gas as well as the applied pressure gradient are known with reasonable accuracy. The model size is controlled by changing the number of nodes in the network. The flow experiment is repeated with larger models until the estimated permeability reaches a constant value. The volume used for the stabilized permeability value is the representative elementary volume (REV) that can be defined for this network system. Since the pore throats of the pore network experiences the transport mechanisms identified using molecular simulation of flow in organic capillary, the predicted REV is also a reasonable representation of the mature organic material associated with the source rocks.

A sensitivity analysis was carried out using the quantities listed in Table 1 to investigate the role of different parameters such as pressure, pressure gradient, throat size, and pore size on the REV. Among them the throat size distribution is found to be the major factor influencing the volume as shown in Figure 3, where permeability is obtained at fixed pressure, pressure gradient, and coordination number. Log-normal distribution was used with varying mean values. Hence, the average size of the throats is the only variable in Figure 3.

ore network properties	
$R_{throats}$, nm	2, 4, 6 and 8
R_{pores}, nm	25 ± 20
c_{om}, psi^{-1}	6×10^{-6}
Adsorption parameters & Gas properties	
P_L, psi	1500
V_s, SCF/ton	100
D_k, nm^2/s	$f_1(r_p,T)$
D_s, nm^2/psi-s	5×10^{-12}
Viscosity, poise-s	$f_2(P,T)$
z	$f_3(P,T)$
Boundary and initial conditions	
P_i, psi	250 - 5,000
$\Delta P_{outlet-inlet}$, psi	10
P_c, psi	P_i x (1.15/0.35)
Temperature, R	745

Table – 1: Design parameters for Figure 3

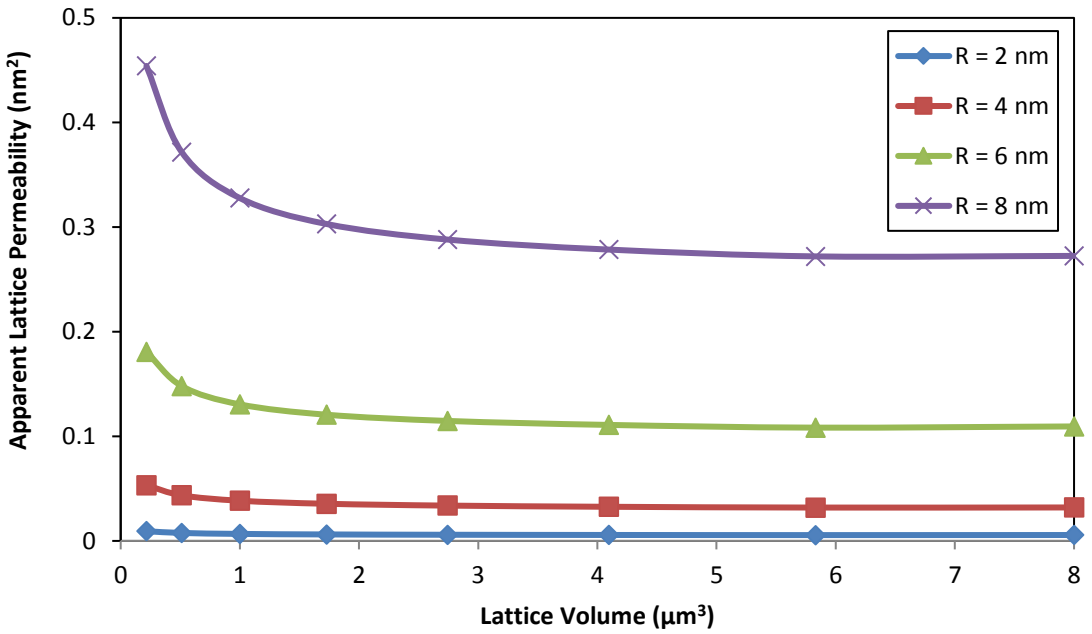

Figure 3 – Sensitivity analysis showing that the REV is only influenced by the average throat size, R.

2.3 Sensitivity Analysis on the Apparent Permeability

Carefully evaluating the terms that appear in the governing equations of the pore network model, I determine that some terms in the algebraic equations are pressure dependent such as the Knudsen diffusion effect (*i.e.* D_k/P), the adsorbed and free phase density values, and the gas viscosity. This implies a strong correlation between rate of gas flow rate and pressure. Hence, the pressure within the system would affect the permeability of the system. In other words, the organic material permeability in the source rocks is expected to be a dynamic quantity rather than an intrinsic property of the rock.

Therefore, my sensitivity analysis using the organic nanopore network model should comprise of two parts. The first one is related to the factors pertaining to the intrinsic part of the permeability such as the pore and throat sizes distributions, pore network coordination number, directional flow paths and heterogeneity. In some references, this part of the permeability is referred to as the liquid or absolute permeability indicating that it is independent of the fluid being transported through the rock. However, the size distribution would also influence the dynamic part of the permeability as can be inferred from the second and third terms of the single capillary equation.

Coordination number of the network is another factor that is related to the intrinsic permeability of the organic material. Value of the coordination number greater than 6 would mean the presence of interconnecting pores in different planes which reduces the directional heterogeneity in the model. Note that six is the maximum number of interconnected throats along the same plane in my model. There is a well-established methodology in the literature discussing the absolute permeability of rocks with all factors influencing it (O'Carroll et al. 1993). In my sensitivity analysis, the main goal is to study the deviation of organic material permeability from its absolute value due to the mechanisms of adsorption and diffusion.

The adsorptive-diffusive portion of the organic material permeability would be dictated by some factors including the pore pressure which directly affects the Knudsen diffusion as well as it affects the adsorbed phase mobility through the density ratio, which appears in the adsorbed phase mobility term of the single capillary equation. In

addition to the pore pressure, the sizes of the throats would also influence the diffusive terms as mentioned previously. Unlike the case of single-capillary, where one deals with only the diameter of the capillary, the pore network model consists of a distribution of throat radii which will be investigated in the sensitivity analysis by considering a different distribution.

A case study is designed to study the effect of the pressure. All parameters were fixed and the average pore pressure within the pore network model was varied in between 250-5,000psi as listed along with the other parameters in Table 2.

Pore network properties	
$R_{throats}$, nm	5 ± 2
R_{pores}, nm	25 ± 5
c_{om}, psi^{-1}	6×10^{-6}
Adsorption parameters & Gas properties	
P_L, psi	1500
V_s, SCF/ton	100
D_k, nm^2/s	$f_1(r_p,T)$
D_s, nm^2/psi-s	5×10^{-12}
Viscosity, poise-s	$f_2(P,T)$
z	$f_3(P,T)$
Boundary and initial conditions	
P_i, psi	250 - 5,000
$\Delta P_{outlet-inlet}$, psi	10
P_c, psi	P_i x (1.15/0.35)
Temperature, R	745

Table – 2: Design parameters for figure 4

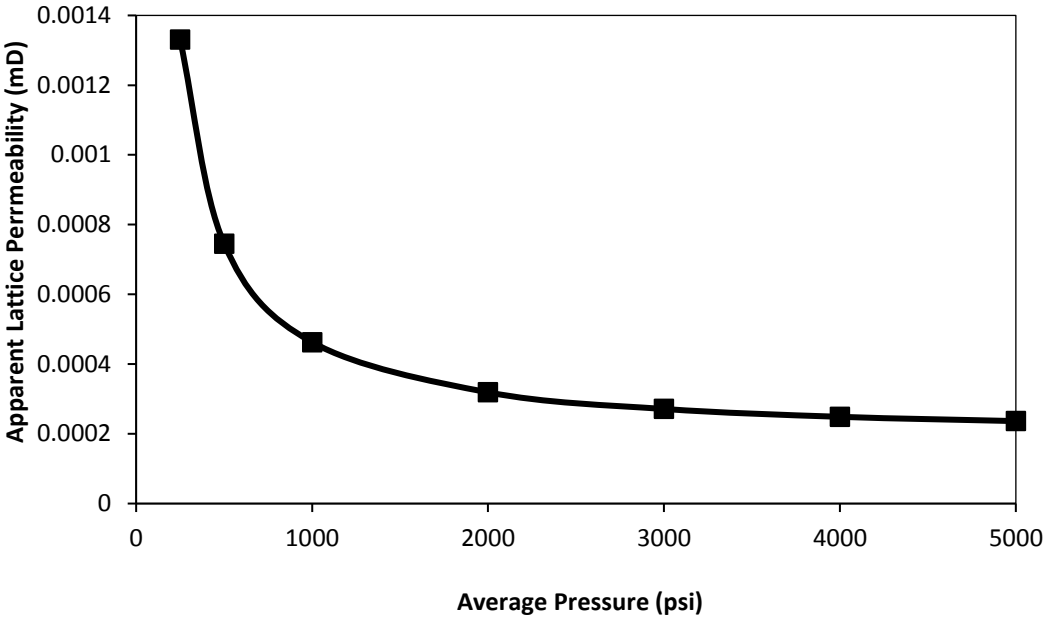

Figure 4 —Organic material apparent permeability as a function of average pore pressure.

The results are shown in Figure 4 and indicate a pressure-dependent gas transport where the apparent permeability is largest at low pressure values, decreases dramatically at average pore pressure values less than 1,000psi, and decreases gradually as the pore pressure in the network is increased further. This type of permeability behavior is well-known for very tight formations because at low pressure, the Knudsen diffusion is relatively high and dominates the overall transport. Moreover, there is an additional mechanism in my case, which is the cluster diffusion of the adsorbed molecules by the walls of the organic material. In order to quantify its magnitude, I repeated the same analysis without the adsorbed phase mobility term of the governing single-capillary equation as shown in Figure 7.

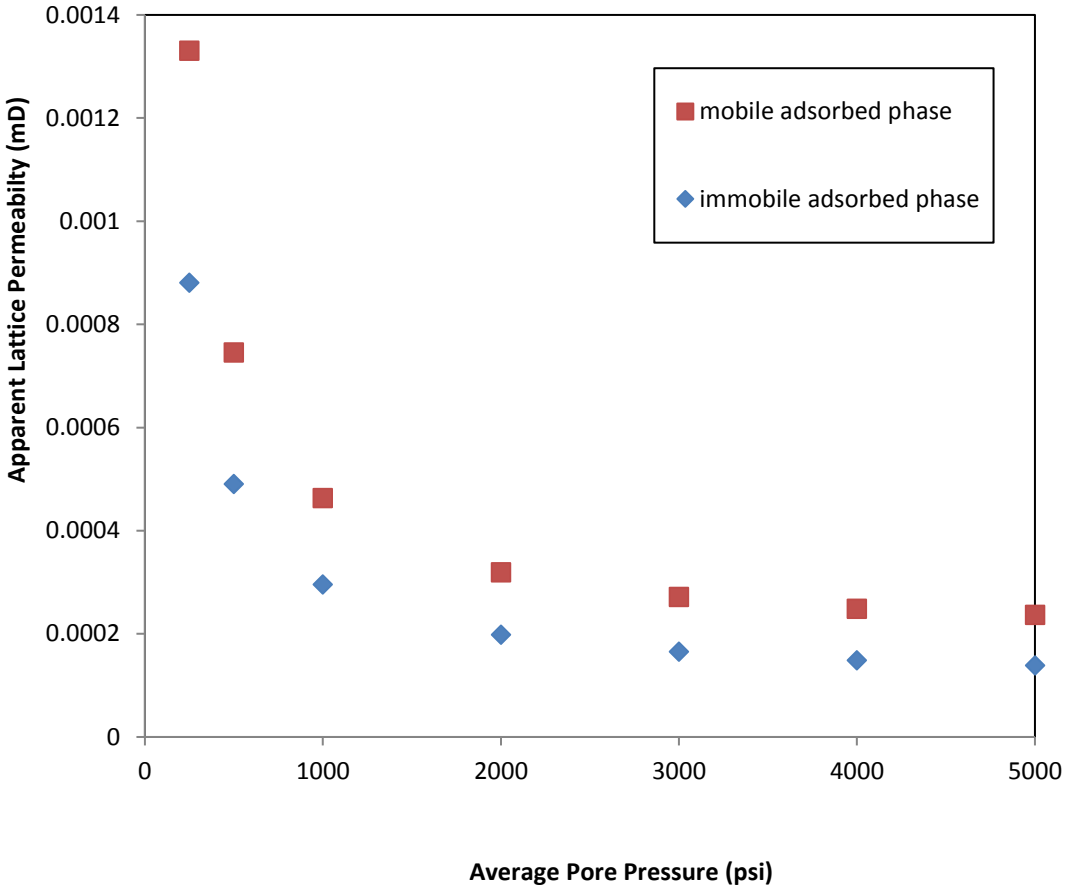

Figure 5 — Apparent permeability of the as a function of pressure when the adsorbed phase is considered immobile and mobile.

From Figure 5, it can be seen that ignoring the cluster diffusion by the surfaces of the organic nano-capillaries would result in underestimating the apparent permeability by 50% at low pressure and around 30% at high pressures for this specific case given in Table 2. The result shows the significance of considering this mechanism under certain conditions of pore sizes and reservoir pressure.

The second factor I investigated as part of my sensitivity analysis is the throat size distribution. The goal is to investigate up to what extent varying the effective throat size would influence the apparent permeability of the pore network. All other parameters were kept constant except the mean size of the distribution. The analysis is performed for some range of throat distribution variances as listed in Table 3.

Pore network properties	
$R_{throats,\ avg}$, nm	2 to 30
Variance	0.1 to 0.7
R_{pores}, nm	25 ± 5
c_{om}, psi^{-1}	6×10^{-6}
Adsorption parameters & Gas properties	
P_L, psi	1500
V_s, SCF/ton	100
D_k, nm^2/s	$f_1(r_p,T)$
D_s, nm^2/psi-s	5×10^{-12}
Viscosity, poise-s	$f_2(P,T)$
z	$f_3(P,T)$
Boundary and initial conditions	
P_i, psi	1,000
$\Delta P_{outlet-inlet}$, psi	10
P_c, psi	P_i x (1.15/0.35)
Temperature, R	745

Table – 3: Design parameters for Figure 6

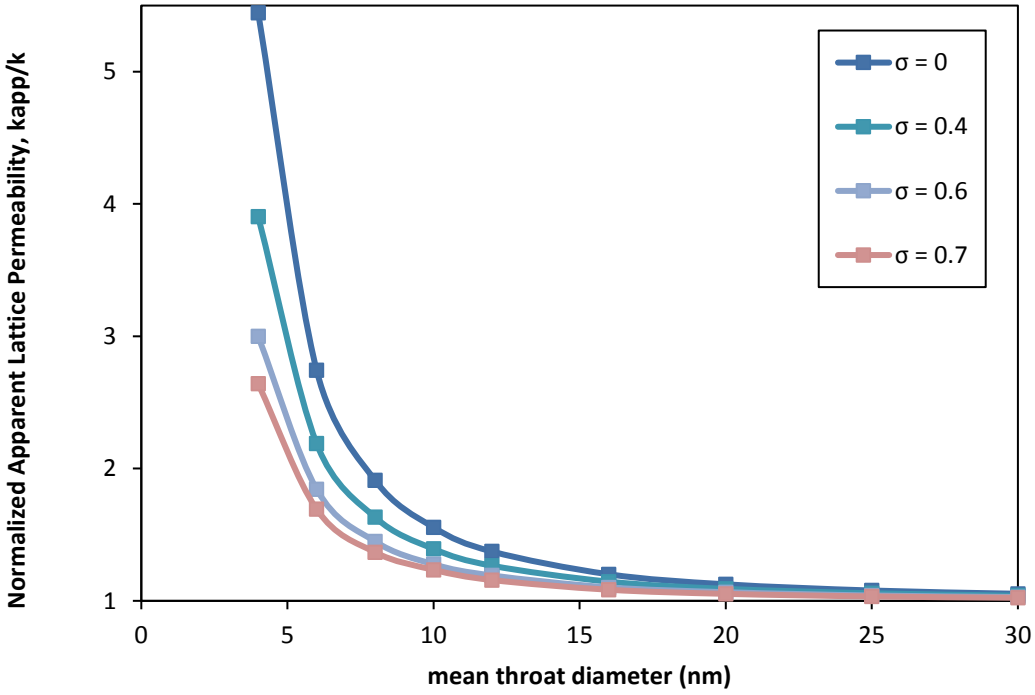

Figure 6 – Apparent permeability ratio as a function of throat mean diameter and range of log-normal variance values at fixed pore pressure of 1,000psi. Here *k* is the absolute or intrinsic permeability of the lattice.

The ratio between apparent and absolute permeability values shown in Figure 6 is sensitive to the effective size of the throats in the organic nanopore network model. As the effective size is reduced to a value below 10nm, the overall transport becomes adsorptive-diffusive in nature. This, in turn, leads to a significant enhancement in the apparent permeability. If the pressure is further reduced below 1,000 psi, the permeability ratio is expected to be even higher.

Changing the variance of the throat size distribution has also some impact on the permeability ratio. As the variance is increased, the likelihood of sampling larger size throats is increased. I have found that the effect of sampling larger capillaries, however, can be negligible for coordination number below 6. At a small coordination number, although they may exist as part of the network, the large capillaries are kept isolated and, hence, their impact on the total flow rate is insignificant. However, these large capillaries are more likely to be connected and dominate the total flow rate at higher coordination numbers.

It is worth mentioning that the selected distribution type in this case is log-normal distribution which is more of an idealized scenario. That was done for the purpose of directly relating the effective size to the mean size of the distribution. However, this might not be case when the distribution of the organic matrix is multi-modal. That would require more analyses to obtain the effective capillary size of the global pore network system.

Based on our sensitivity analysis, there are two main factors that must be carefully evaluated in order to define the apparent organic material permeability. These two factors are the average pore pressure and the effective capillary size. These will determine the degree of change in the apparent permeability from its absolute value.

2.4 Effective Capillary Size*

A scaled up permeability for the kerogen pore network including adsorption and diffusion effects can be determined based on a characteristic capillary size of the network. For some types of distributions such as normal and log-normal, the average radius can be taken as the characteristic size. However, for other types of irregular distributions such as multi-modal distribution, the average radius may not be the characteristic size. In the latter case, percolation theory can be used to find out the characteristic nano-capillary size for permeability. In a general porous medium from inlet to outlet, percolation threshold represents the extent of the long-range (system-size spanning) connectivity in the medium. Below that threshold, no connectivity exists.

Percolation threshold is related to percolation radius as follows:

$$P_c = \int_{R_P}^{R_{max}} r\, f(r)\, dr \qquad (5)$$

where $f(r)$ is the capillary size distribution of the porous medium, R_{max} the largest size in that distribution, and R_P the percolation radius at the percolation threshold. For a direct application in the pore-network modeling approach, this could be interpreted as follows. Initially, eliminate the connectivity in the network completely by switching off all of the throats in the network. Next, connect the throats in the network in a systematic way size-by-size starting with R_{max} in descending order until the long-range connectivity between inlet and outlet of the lattice is formed. The capillary size at which the long-range

* Reprinted with permission from "Matrix-Fracture Interactions during Flow in Organic Nanoporous Materials under Loading" by Saad Alafnan & Yucel Akkutlu, 2017. Journal of Transport in Porous Media.

connectivity has just established is referred to as the percolation radius. P_c is called the threshold of the system (O'Carrol et al. 1993).

The percolation radius can be thought of as a characteristic size of the system and used to estimate the upscaled or apparent permeability of the capillary network.

2.5 Apparent Permeability Formula

The general apparent permeability formulation for the organic nanoporous material should take into account the previously discussed three transport mechanisms, which are viscous flow and the adsorptive-diffusive transport. In many publications, the diffusive portion of permeability of very tight formation is dealt with as a factor multiplied by the absolute permeability. An example of that is the well-known Klinkenberg equation (Klinkenberg 1941):

$$k_{app} = k\left(1 + \frac{b_k}{P}\right) \qquad (6)$$

where, k is the absolute permeability and $(1+b_k/P)$ is the multiplier correcting for the diffusive nature of the transport which is significant for very tight formations. In my case, I have an additional flux term coming from the presence of the mobile adsorbed phase.

The adsorbed layer does not only act as an additional mechanism but it also affects the viscous and diffusive flow because of the space it occupies. This effect has been considered at the microscopic level. Revisiting equation 2 which models the

viscous-adsorptive-diffusive flow in the single organic capillaries, the radius of the capillary is corrected for the presence of the adsorbed layer. The same correction is needed when writing the organic materials apparent permeability formula at the macroscopic scale.

Therefore, the apparent permeability for the organic pore network could be written in this form:

$$k_{app} = k\left(R^* + \frac{b_k}{P} + a\right) \qquad (7)$$

where, R^* is the correction factor for the viscous flow accounting for the presence of the adsorbed layer and its value is between 0 when the whole pore space is taken by the adsorbed layer, and 1, when there is no adsorbed layer at all. b_k/P and a are the coefficients of the Knudsen diffusion and adsorbed phase mobility, respectively, which are fixed at a given pore pressure and effective throat radius.

These three coefficients can be obtained by relating the microscopic single capillary equation to the macroscopic apparent permeability model using the concept of the percolation theory. In other words, apparent to absolute permeability ratio is the same as the ratio of viscous single capillary equation given by Hagen Poiseuille to its modified form (*i.e. equation 2 which includes all three flow mechanisms*) at a throat size representing the whole network. That size is the percolation radius:

$$\frac{k_{app}}{k} \approx \frac{q_{Percolation\ radius}}{q_{HP,Percolation\ radius}} \tag{8}$$

$$\frac{q_{Percolation\ radius}}{q_{HP,Percolation\ radius}} = \frac{r_{P,\,ads}^4}{r_P^4} + 8\mu D_K \frac{1}{P}\frac{r_{P,ads}^2}{r_P^4} + 8\mu \frac{\rho_s}{\rho}\frac{D_s}{r_P^2}\frac{\left(r_P^2 - r_{P,ads}^2\right)}{r_P^2} \tag{9}$$

$$k_{app} = k\left(\frac{r_{P,\,ads}^4}{r_P^4} + 8\mu D_K \frac{1}{P}\frac{r_{P,ads}^2}{r_P^4} + 8\mu \frac{\rho_s}{\rho}\frac{D_s}{r_P^2}\frac{\left(r_P^2 - r_{P,ads}^2\right)}{r_P^2}\right) \tag{10}$$

In equation (10) the flow transport factors are introduced:

$$R^* = \frac{r_{P,\,ads}^4}{r_P^4} \tag{11}$$

$$b_{kn} = 8\mu D_K \frac{1}{P}\frac{r_{P,ads}^2}{r_P^4} \tag{12}$$

$$a = 8\mu \frac{\rho_s}{\rho} \frac{D_s}{r_P^2} \left(\frac{r_P^2 - r_{P,ads}^2}{r_P^2} \right) \qquad (13)$$

where, r_P and $r_{P,ads}$ are the percolation radius and the percolation radius corrected for the thickness of the adsorbed layer, respectively.

2.5.1 Case Study

In order to explain how percolation theory can be related to pore network modeling and to describe the transport within the organic material, the following example is given. Pore network model is built as described in the first part of Section 2 with its pore and throat sizes being sampled from the distributions given in Figure 7. The other design parameters are given in Table 4.

After constructing the pore network model, several apparent permeability measures are obtained as a function of pressure. Now, the apparent permeability results are to be compared against those obtained by equation 10 whose coefficients are being evaluated at the percolation radius and at the average pore pressure. The first task is to obtain the absolute permeability and that can be achieved by simply running the pore network model using an inert liquid as the measurement fluid in order to eliminate the diffusive-adsorptive fluxes. After that, the percolation radius is obtained numerically by switching off all the capillaries and then opening them one by one starting with R_{max} in descending order. The throat size at which the fluid ceases to flow is the percolation radius.

Pore network properties	
R_P, nm	Given in figure 7
R_{pores}, nm	30 ± 10
c_{om}, psi^{-1}	6×10^{-6}
Adsorption parameters & Gas properties	
P_L, psi	1500
V_s, SCF/ton	100
D_k, nm^2/s	$f_1(r_p,T)$
D_s, nm^2/psi-s	5×10^{-12}
Viscosity, poise-s	$f_2(P,T)$
z	$f_3(P,T)$
Boundary and initial conditions	
P_i, psi	250 - 5000
$\Delta P_{outlet-inlet}$, psi	10
P_c, psi	P_i x (1.15/0.35)
Temperature, R	745

Table – 4: Design parameters for the case study of determining organic pore network apparent permeability using percolation theory

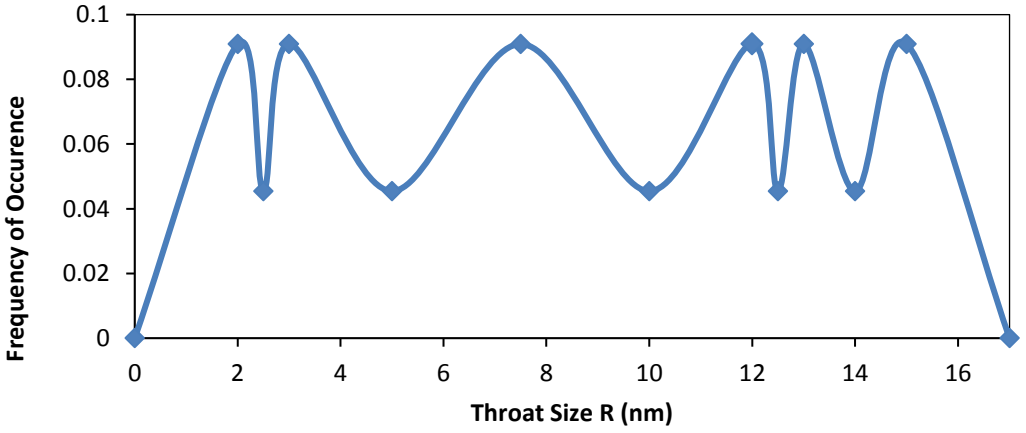

Figure 7 – Throat size distribution used to investigate the percolation theory and the organic materials apparent permeability model

It is important to notice that there is no direct relationship between size distribution and percolation radius because additional factors such as the coordination number and the local heterogeneity could also play an important role in determining the percolation radius.

In general, the higher the coordination number, the more likely the large-size capillaries will be interconnected and, hence, contribute to the flow. Large values of the coordination number would shift the percolation radius more towards the right hand side of a distribution (*i.e.* r_P *would be closer to* R_{max}).

In Figure 8, I provide a general work flow of how pore network modeling can be used to obtain the percolation radius associated with the network permeability.

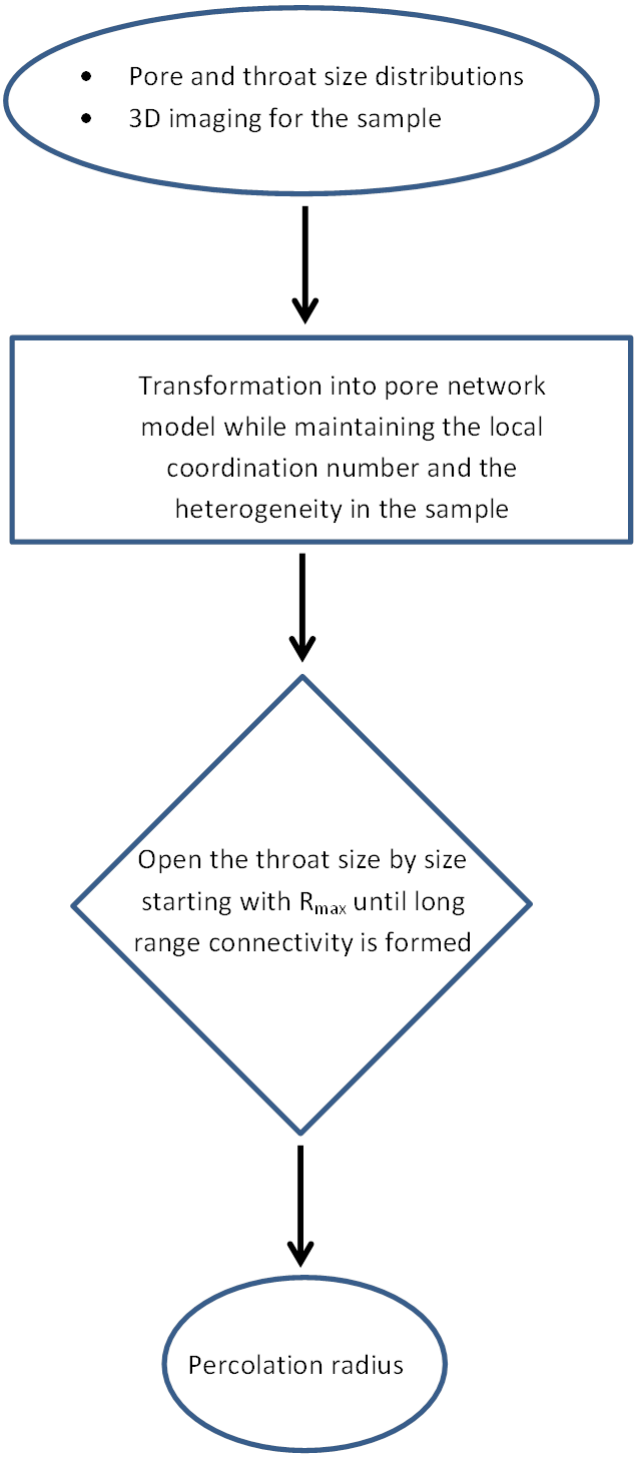

Figure 8 – Workflow summarizing procedure to determine the percolation radius using throat size distributions, 3D imaging, and pore network modeling.

The percolation radius in this particular case is approximated to be somewhere in between 12 and 13 nm based on the methodology explained in Figure 8. Next, this radius is corrected for the presence of the adsorption layer using the Langmuir isotherm (*i.e. Langmuir isotherm model is based on the assumption of monolayer*) which is equivalent to the kinetic diameter of single methane molecule.

The transport coefficients given by equations 12, 13, and 14 were evaluated based on the value of the percolation radius and for a range of pressure values between 200 to 6000 psi.

Using the estimated value of absolute permeability and the diffusive transport coefficients, the organic apparent permeability is estimated and plotted in Figures 9 against those obtained directly from the pore network model. For comparison, the same permeability analysis is repeated when the flow coefficients are evaluated at the mean value of the throat size distribution, which is 8 nm, as shown in Figure 10.

As can be seen from the two cases, the apparent permeability estimation is very sensitive to the effective radius used for its estimation especially at the lower range of pressure values where the overall transport is controlled by diffusive-adsorptive mechanisms.

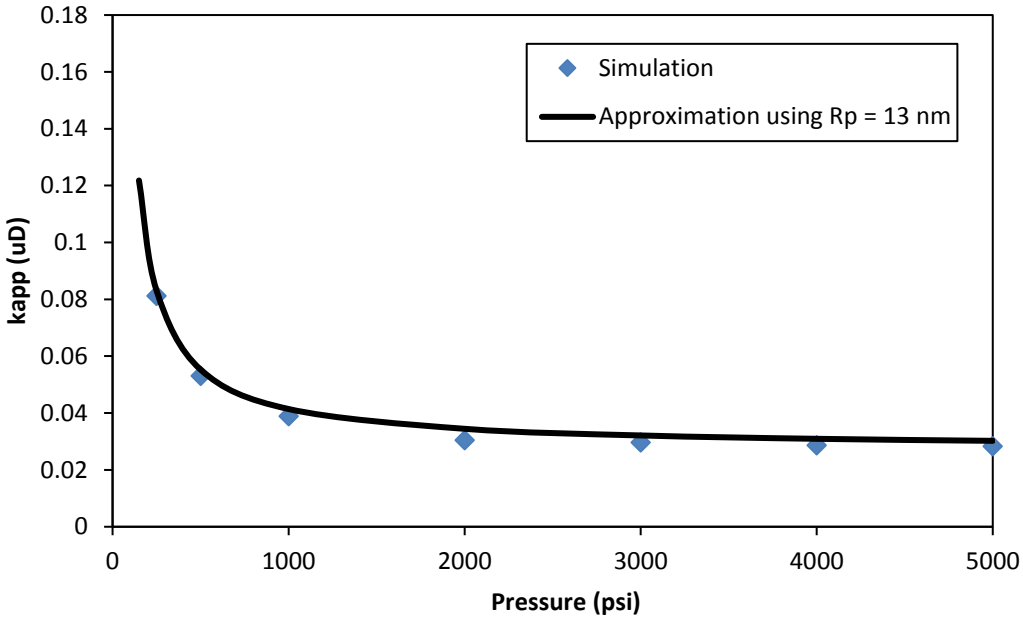

Figure 9 – Apparent permeability approximation for the organic pore network at the percolation radius.

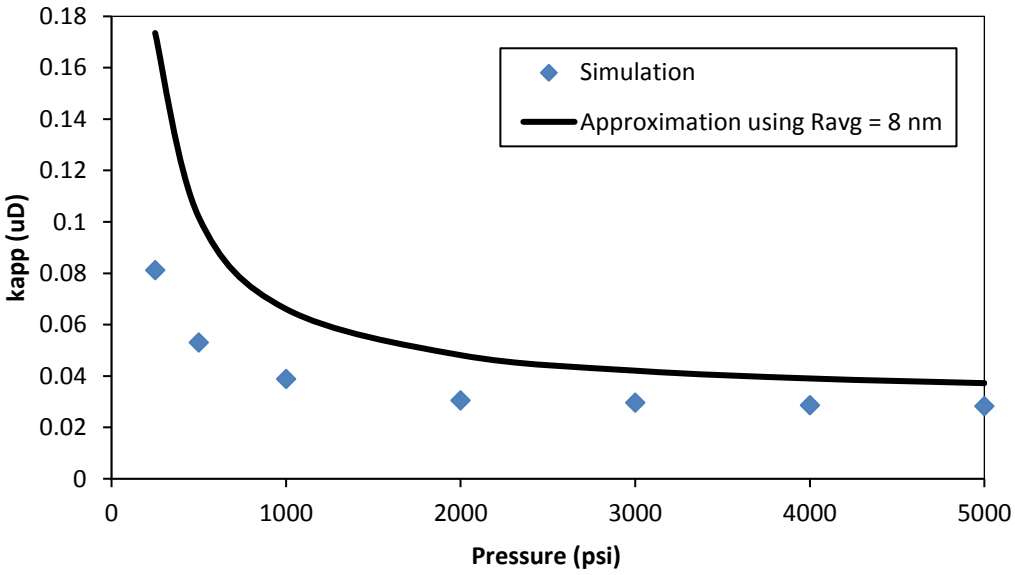

Figure 10 – Apparent permeability approximation for the organic pore network at the mean value of throat size distribution.

2.6 Flow Regimes

As discussed in the previous sections, viscous-diffusive mechanisms coexist in the transport within the organic materials of shales with each one of them prevails at certain conditions of reservoir pressure and capillary size distributions. My interest is to predict the mode of gas transport at given conditions. Therefore, the concept of dimensionless numbers is used to evaluate the relative importance of one mechanism over the others at some predefined conditions.

Péclet number is defined as the ratio of convection to diffusion. Moreover, mass transfer Biot number is used to predict the ratio of surface diffusion to free molecular diffusion (*i.e. adsorptive diffusion to Knudsen diffusion*). Those two numbers can be used to characterize the flow mechanisms in the organic materials.

$$N_{Pe} = \frac{\text{Viscous flow}}{\text{Knudsen diffusion}} \qquad (14)$$

$$N_{Bi} = \frac{\text{Adsorptive diffusion}}{\text{Knudsen diffusion}} \qquad (15)$$

Again, the concept of percolation theory is invoked to estimate these numbers. Equation 2 for the single-capillary can be divided into three terms. The first one is the viscous, the second is Knudsen diffusion, and the third is cluster diffusion. Each term of the three is written independently and then is evaluated at the percolation radius.

Therefore, the two dimensionless numbers can be written in terms of gas properties and percolation radius as:

$$N_{Pe} = \frac{\frac{1}{8\mu} r_P^4}{\frac{D_k}{P} r_P^2 + D_s \frac{\rho_s}{\rho}\left(r_P^2 - r_{P,ads}^2\right)} \tag{16}$$

$$N_{Bi} = \frac{D_s \frac{\rho_s}{\rho}\left(r_P^2 - r_{P,ads}^2\right)}{\frac{D_k}{P} r_P^2} \tag{17}$$

N_{Pe} values greater than one indicates viscous-controlled transport behavior. That happens at large values of percolation radius (*i.e.* $r_P > 30\ nm$). On the other hand, N_{Pe} less than one would indicate a diffusive mechanism and Biot number can then be used to characterize the relative importance of the diffusion over the adsorptive flow.

$$\text{Dominant Transport Mechanism} = \begin{cases} \text{Convection} & ; \ N_{Pe} \sim \infty \\ \text{Pore Diffusion} & ; \ N_{Pe} \sim 0 \ \text{ and } \ N_{Bi} \sim 0 \\ \text{Cluster Diffusion} & ; \ N_{Pe} \sim 0 \ \text{ and } \ N_{Bi} \sim \infty \end{cases} \tag{18}$$

The significance of introducing these numbers can be emphasized by considering the following example of pore network model with its designed parameters being the same as in the previous example except that we consider two cases of different throat size distributions to investigate the sensitivity of the above dimensionless numbers to the change in capillaries sizes. The percolation size of the first case is 3 nm and the second one is of size 10 nm.

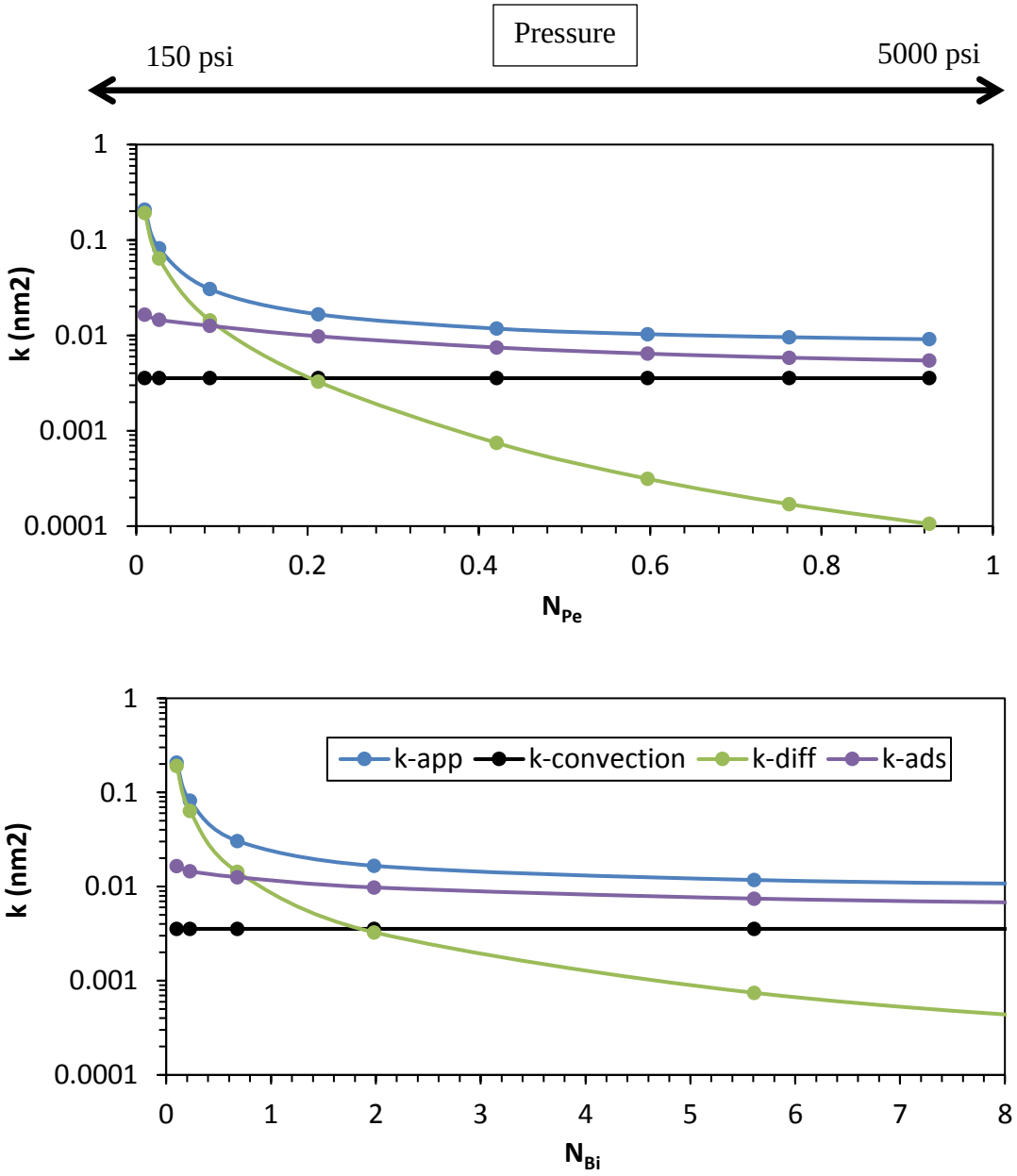

Figure 11 – Péclet and Biot numbers estimated for the organic pore network using a lognormal throat distribution with an average size of 3nm.

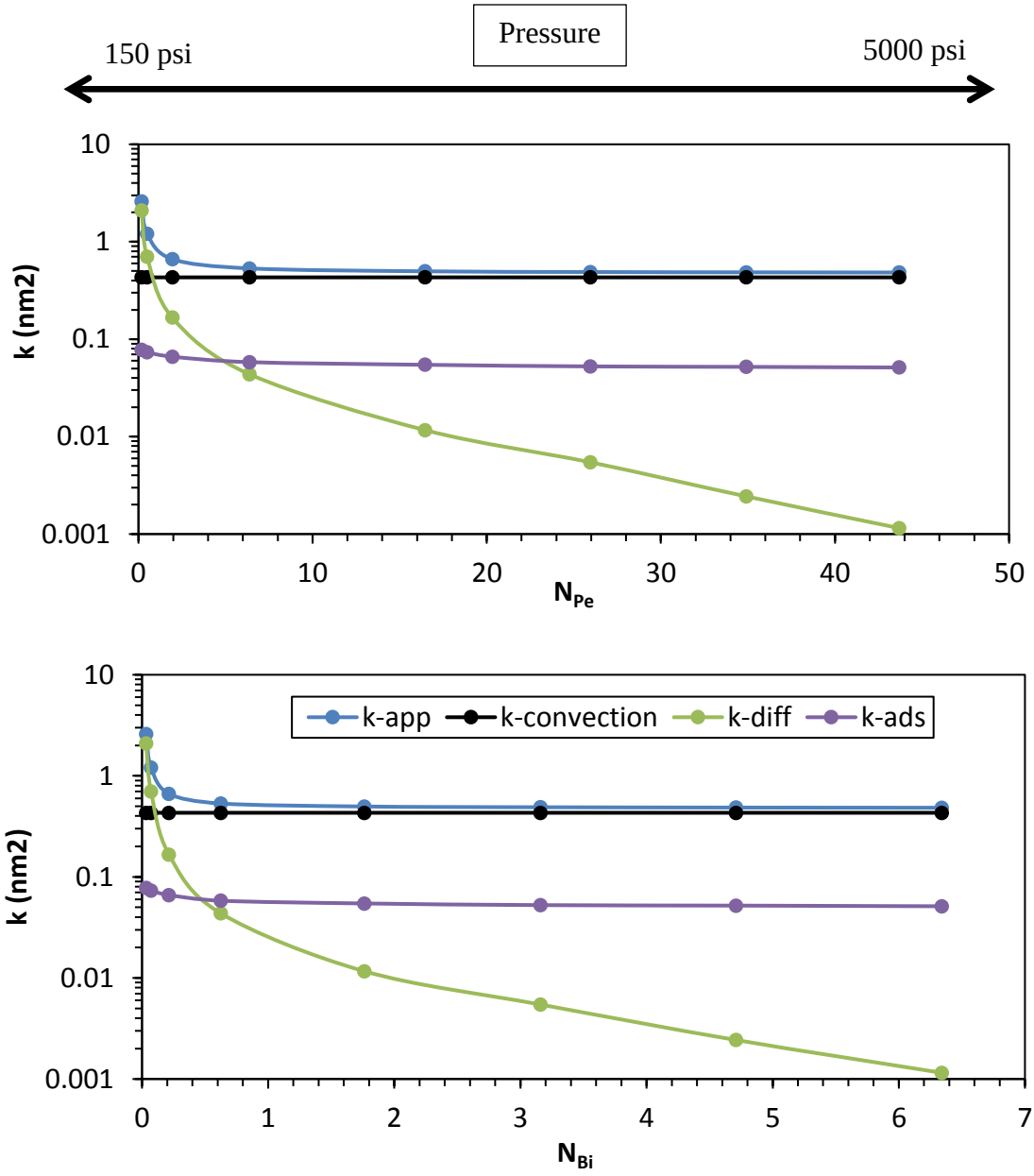

Figure 12 – Péclet and Biot numbers estimated for the organic pore network using a lognormal throat distribution with an average size of 10nm.

For each distribution, the average pore pressure is varied from 150 psi to 5,000 psi and the corresponding apparent permeability components along with the Péclet and Biot numbers are computed. The apparent permeability components are obtained at each run by considering one flow mechanism in the pore network model at a time:

$$q_{tube} = \frac{\pi R_a^4}{8\mu}\frac{dP}{dL} \rightarrow k_{convection} \tag{19}$$

$$q_{tube} = \frac{D}{P}\pi R_a^2\frac{dP}{dL} \rightarrow k_{diffusion} \tag{20}$$

$$q_{tube} = \frac{\rho_{ads}}{\rho_{bulk}} D_s \pi (R_{tube}^2 - R_a^2)\frac{dP}{dL} \rightarrow k_{ads} \tag{21}$$

For the first case where the mean size of the capillary distribution is 3 nm, it was observed that the transport is adsorptive-diffusive even at high pressure values. The Péclet number was below 1.0 for the whole pressure range when the diffusive gas transport was the predominant mechanism. As the pressure is reduced, the adsorptive mechanism started to contribute to the overall flow, which is also reflected on the Biot number values estimated below 1.0.

On the other hand, the 10 nm case shown in Figure 12 (bottom) indicates a transport that is viscous-controlled for the pressure values above 500 psi. At that pressure, the Péclet number has dropped below 1.0 and the transport become equally controlled by diffusion and adsorption.

In general, the diffusive-adsorptive regimes are throat size and pore pressure dependent. They are associated with Péclet number < 1.0. Biot number, on the other

hand, is used to investigate which one of the diffusive mode is more important compared to the other.

The above example relating the Péclet and Biot numbers to the apparent permeability was carried out under steady-state flow condition across the organic pore network. In more realistic shale gas reservoir setting, the gas outflow of the organic material would go through a transient period before reaching to a quasi-steady or steady-state. Therefore, another case is considered where a pore network model representation of the organic material is created with no-flow boundary conditions assumed for all faces of the cube except for one of them, which is the outlet. At that face, a low pressure value is assigned to induce the gas release. The pore network parameters used in the simulation are given in Table 5.

Pore network properties	
R_P, nm	4
R_{pores}, nm	40 ± 10
c_{om}, psi^{-1}	6×10^{-6}
Adsorption parameters & Gas properties	
P_L, psi	1500
V_s, SCF/ton	100
D_k, nm^2/s	$f_1(r_p,T)$
D_s, nm^2/psi-s	5×10^{-12}
Viscosity, poise-s	$f_2(P,T)$
z	$f_3(P,T)$
Boundary and initial conditions	
P_i, psi	7,000
P_{outlet}, psi	500
P_c, psi	P_i x (1.15/0.35)
Temperature, R	745

Table – 5: Parameters used for the simulation of transient gas outflow.

The gas release along with the pressure distribution in the network are obtained. Gas outflux was transformed into a dimensionless flow rate using the following expression:

$$Q_D = q/[P_{avg}^2 - P_{outflow}^2])$$

and plotted versus the time of flow. Additionally, the Péclet number is calculated at each time step using equation 17.

The results shown in Figure 13 indicates a proportionality between Q_D and the Péclet number which is expected because as the network is depleted, the pressure decreases and, in turn,leads to a more diffusive-adsorptive fluxes adding to the overall transport within the organic pore network.

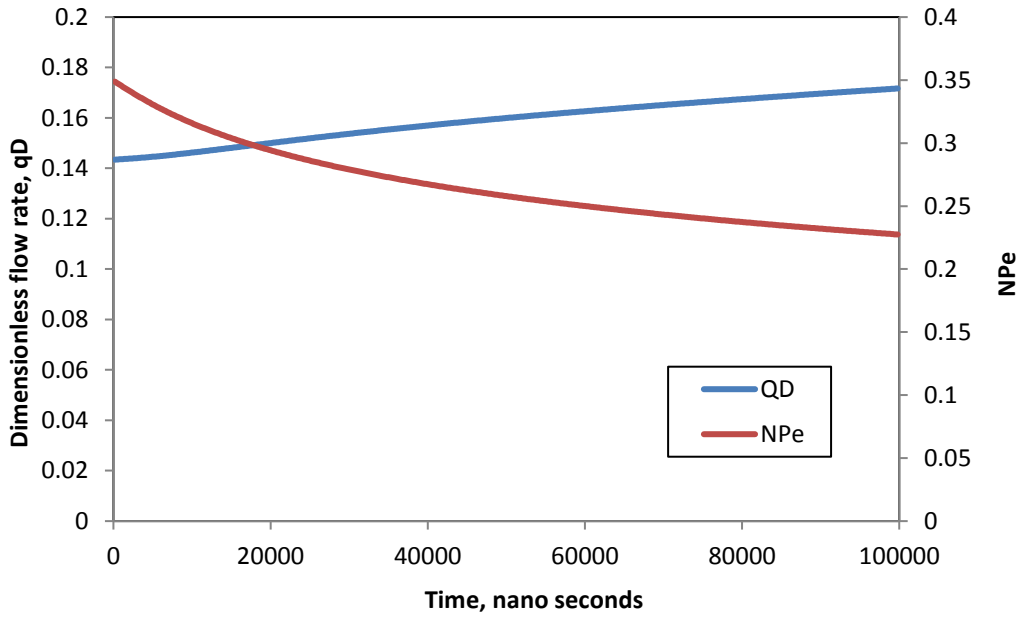

Figure 13 — Transient behavior of the dimensionless flow rate as the organic nano-pore-network is depleted. Note that the transport becomes more diffusive-adsorptive during the pressure depletion.

2.7 Surface Roughness

In the previous section I considered the adsorptive transport in the organic pore network using molecular simulation transport in capillaries with smooth surfaces. Organic materials such as kerogen in the source rocks have pores and capillaries with irregular shapes in most cases, however. These irregularities could lead to some added resistance to the overall transport, due to reduction in the adsorbed phase mobility.

For that reason, I introduced a normalized friction factor as follows:

$$f = 1 - \frac{V_{rough}}{V_{smooth}} \tag{22}$$

Now, the governing single-capillary equation of the pore network model can be modified to account for the friction factor as:

$$q_{modified\,HP} = \frac{\pi R_a^4}{8\mu}\frac{dP}{dL} + \frac{D}{P}\pi R_a^2\frac{dP}{dL} + \frac{\rho_{ads}}{\rho_{bulk}}(1-f)\,D_s\pi(R_{tube}^2 - R_a^2)\frac{dP}{dL} \tag{23}$$

The irregularities that make the surface of the organic material rough do not only cause a resistance to the flow of the adsorbed molecules but also the free molecular diffusion. In the literature, it has been shown that the Knudsen diffusion is also dependent on the wall roughness (Arya et al., 2003 and Levdansky et al., 2007). However, the sizes of the "bumps" in the organic capillaries that cause surface roughness are of the order of magnitude comparable to that of methane molecular size or the methyl group size. Moreover, those molecules tend to adsorb in between sharp edges of the rough surface because these sites are of lower adsorption energy (Panczyk et al.

2008). As a result, molecular collisions that cause Knudsen diffusion will be less influenced by the degree of surface roughness in the organic material.

In the following example, I use equation 23 as the transport in the nano-capillaries which includes the normalized friction factor as the governing equation in the pore network model to study the effect of surface roughness. Pore network simulation runs were made for friction factor values of 0, 0.3, 0.6, and 1. The other designed parameters are given in Table 6. The apparent permeability results were plotted against the reciprocal of pressure for wide range of pressure values starting from 500 psi up to 20,000 psi. Additionally, the simulation results were also compared to those obtained analytically using the formula of the apparent permeability with the friction factor being accounted for:

$$k_{app} = k\left(\frac{r_{P,\,ads}^4}{r_P^4} + 8\mu D_K \frac{1}{P}\frac{r_{P,ads}^2}{r_P^4} \; + (1-f)\, 8\mu \frac{\rho_s}{\rho}\; \frac{D_s}{r_P^2}\; \frac{\left(r_P^2 - r_{P,ads}^2\right)}{r_P^2}\right) \qquad (24)$$

The results are shown in Figure 14.The case of extremely rough surface shows linear relationship with the reciprocal of the pressure. In this case, the absolute permeability can be obtained from the y-intercept using the Klinkenberg's model. However, as the mobility of the adsorbed phase gradually increases, that relationship becomes nonlinear. The y-intercept in that case represents the absolute permeability plus some constant enhancement due to the presence of the adsorbed phase (*i.e. as the pressure is increased, the density ratio of the adsorbed and the free phases approaches to 1.0 which results in a constant adsorbed phase flux*).

Pore network properties	
$R_{throats}$, nm	3 ± 2
R_{pores}, nm	25 ± 20
c_{om}, psi^{-1}	6×10^{-6}
friction factor	0, 0.1, 0.3, 0.6 and 1
Adsorption parameters & Gas properties	
P_L, psi	1500
V_s, SCF/ton	100
D_k, nm^2/s	$f_1(r_p,T)$
D_s, nm^2/psi-s	5×10^{-12}
Viscosity, poise-s	$f_2(P,T)$
z	$f_3(P,T)$
Boundary and initial conditions	
P_i, psi	5,000 to 20,000
$\Delta P_{outlet-inlet}$, psi	10
P_c, psi	P_i x (1.15/0.35)
Temperature, R	745

Table – 6: Design Parameters for surface roughness effect on the apparent permeability

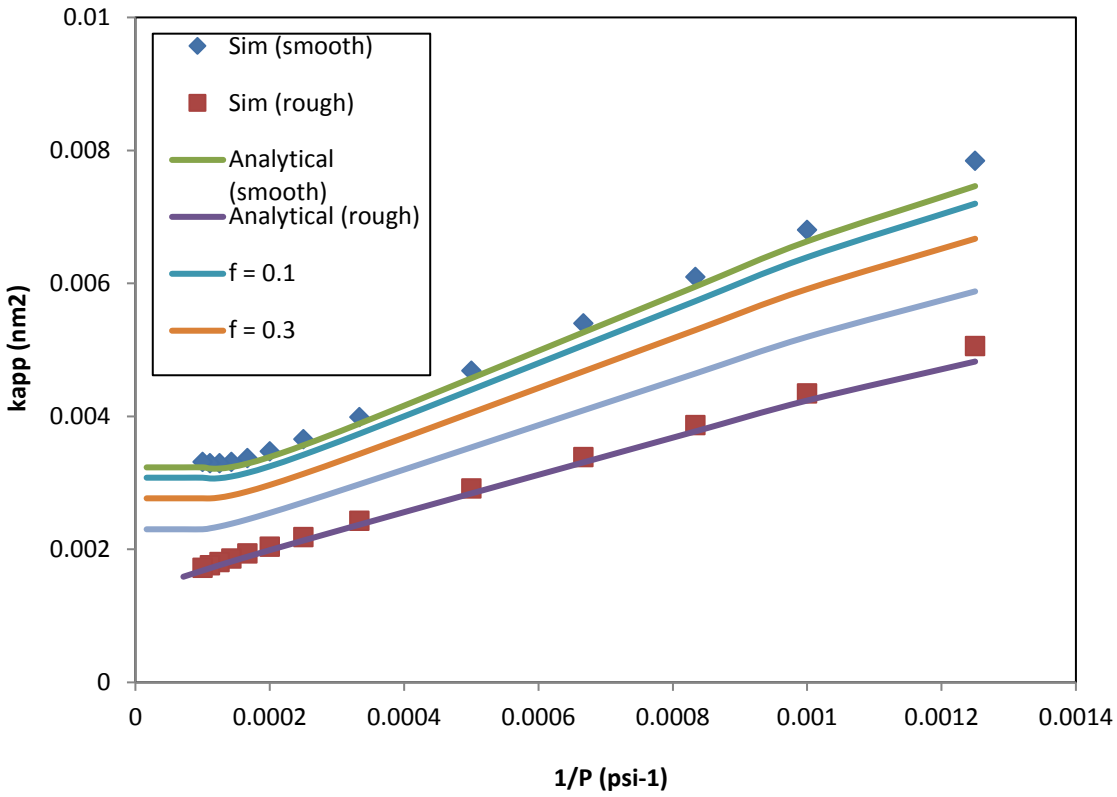

Figure 14 – Apparent permeability of the organic pore network as a function of capillary surface roughness.

2.8 Porosity-Permeability Relationship

In porous media, porosity is related to permeability and their relation includes medium tortuosity, which is the ratio used to characterize the fluid pathways between two points to the straight distance between them. The well-known Kozeny-Carmen porosity-permeability relationship is given as:

$$k = \frac{\emptyset\, r_P^2}{8\,\tau} \tag{25}$$

where, τ is the tortuosity and $\emptyset$ is the porosity. Pore network simulations are carried out assuming only viscous flow, i.e., when Hagen-Poiseuille is the basis of the mass balance and neither diffusion nor adsorption fluxes are included to check the consistency of the network model in relating porosity to absolute permeability. Hence, the tortuosity of the pore network system can be obtained. The design parameters of the network model are the same as the ones given earlier in Table 3 except that the variance is now kept constant at a value of 0.5. Linear relationship between the absolute permeability and the porosity is found indicating that the network model is working properly. The tortuosity of the system is obtained from the slope as 1.5.

Next, the simulations are repeated using equation 2 as the basis of mass balance. The surface roughness was taken as a constant and equals to zero. In this case, the Kozeny-Carmen relationship is nonlinear especially at low values of the percolation radius and yields a much smaller tortuosity value of 1.25, see Figure 15, Left.

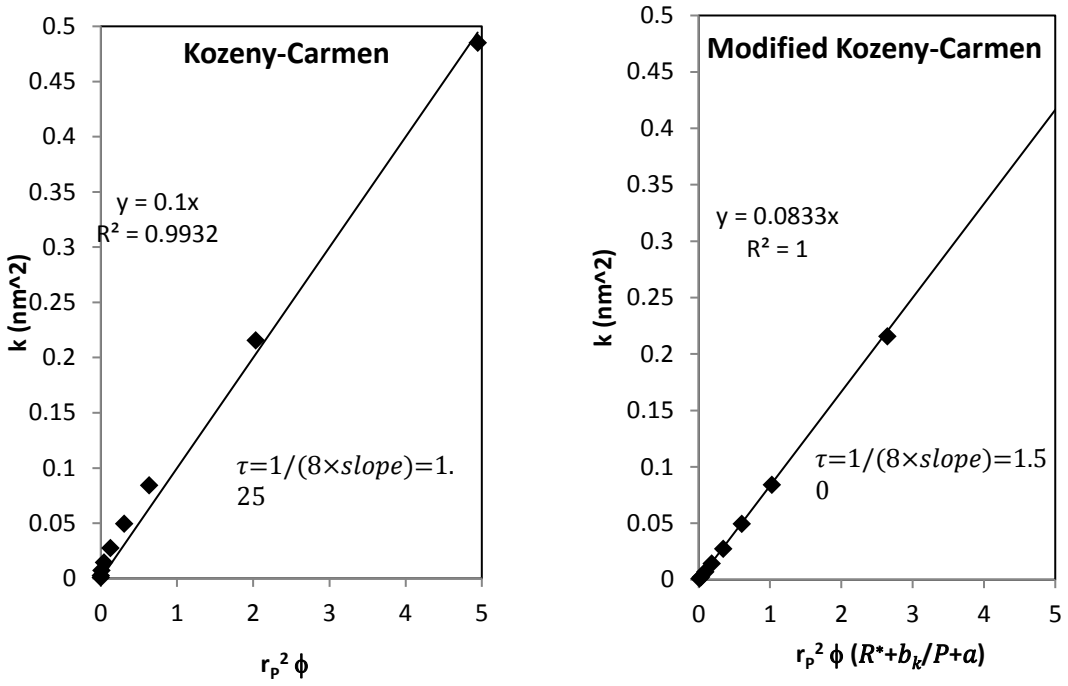

Figure 15 – Porosity-permeability relationship for organic materials using Kozeny-Carmen relationship and the modified one.

The Kozeny-Carmen relationship can be modified by accounting for the diffusive-adsorptive mechanisms as follows:

$$k = \frac{\emptyset\, r_P^2}{8\,\tau}\left(R^* + \frac{b_k}{P} + a\right) \tag{26}$$

The proposed modified equation is checked using the pore-network simulation results, Figure 15, Right. Indeed, when the correction is included, the actual tortuosity value of the network is now recovered, indicating the importance of accounting for the adsorptive-diffusive transport mechanisms in petrophyscial analysis of the organic-rich source rocks.

3. NANOPOROUS ORGANIC MATERIAL-CRACK INTERACTIONS

3.1 Multiscale Pore Network Model for Gas Transport in Shale

Building a representative pore network model of organic materials and their associated cracks would require dealing with length scales of different order of magnitudes. The organic pores are of nanoscale size while the cracks have much larger sizes. The concept of integrated pore network model can be used in this case where each network is built independently and then integrated into a selected domain which can be the domain of the larger length-scale or subdomain of it (Butler et al., 2016).

In our case, the organic material pore network model is the same as the one described in Section 2.1 while the model of crack is considered to be a channel in a rectangular shape. The two domains are integrated into a nested structure as shown in Figure 16.

In the channel representing the crack, the mass conservation is the same as the one in equation 4 with the flux term given by Stoke's flow equation in rectangular channel:

$$Q = \frac{h^3 w}{12\,\mu}\frac{\Delta P}{L} \qquad (27)$$

where, h and w are the hight and width of the channel.

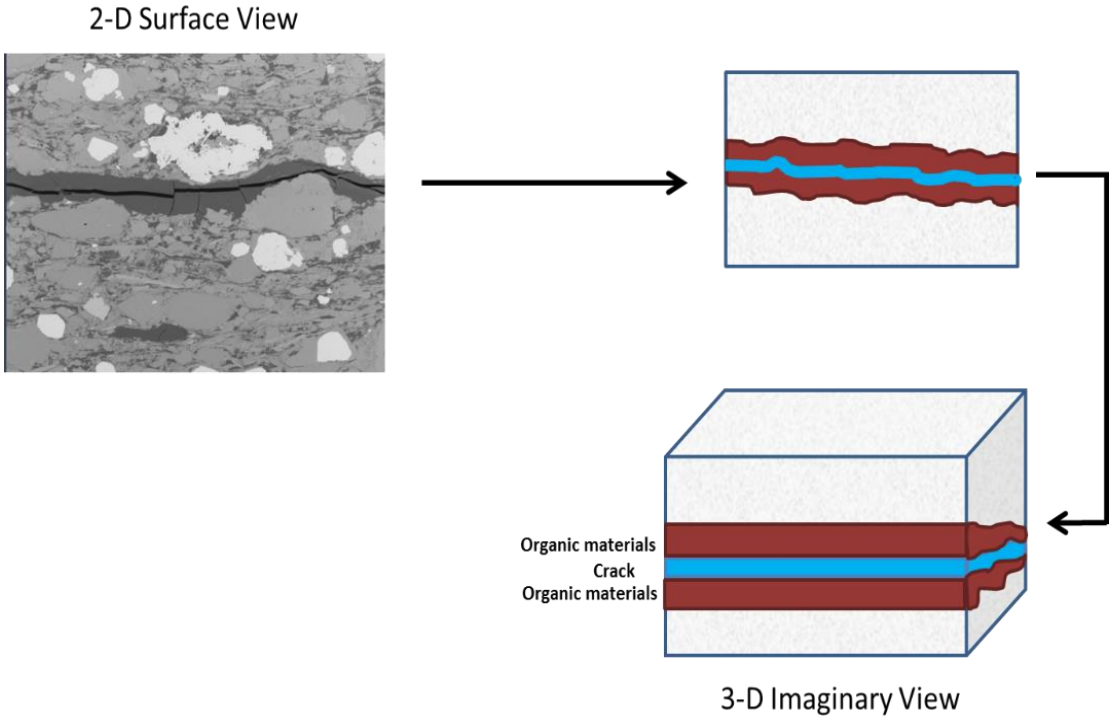

Figure 16 – Conceptual model used in building the multi-scale pore network model including a rectangular shape micro-crack.

3.2 Interactions of Organic pore Network with Crack

In this section of the dissertation, the interactions between the organic pore network that was studied in the previous sections and the crack associated with them are investigated via a multi-scale pore network modelling approach. The structure of the multi-scale network model was described in the second part of Section 2. The conceptual model depicted in Figure 17 consists of the organic pore network model and a crack of a size that is of larger size. Additionally, the governing flow equations in both media are

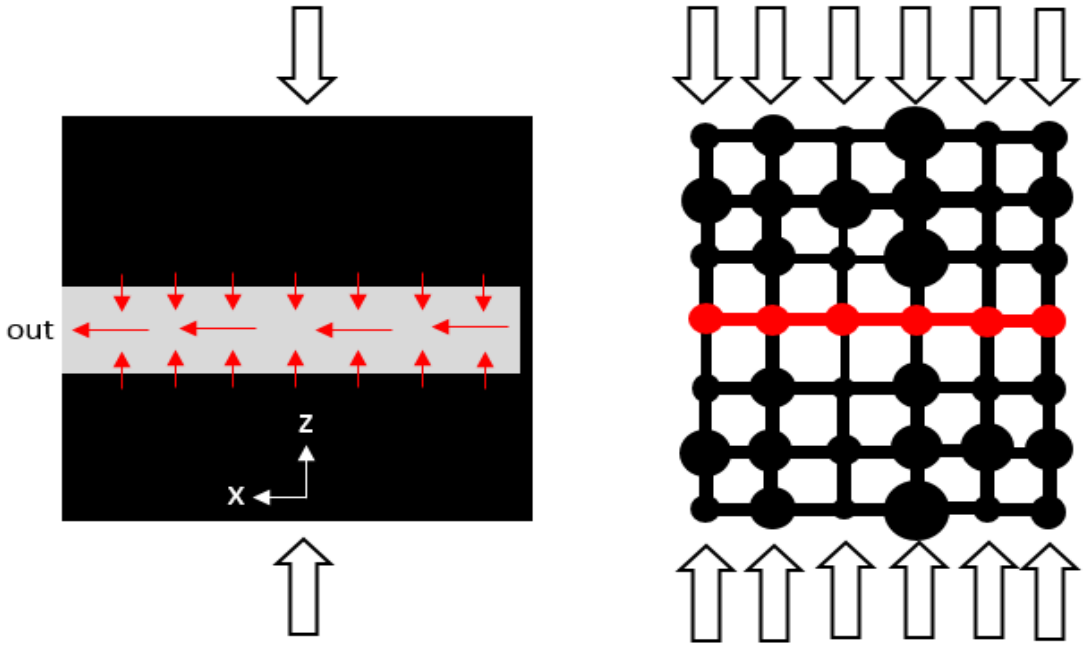

Figure 17 — LEFT: 2D representation of 3D nanoporous organic material with a crack. Fluid is released from the nanoporous organic matrix into the fracture and relased. The crack width is allowed to change over time due to external load working on the system. RIGHT: 2D representation of 3D pore network model representing the organic pore network and the crack with nano-scale capillaries.

different. The flow in the crack is pressure gradient-induced viscous flow, while it is of convective-diffusive-adsorptive nature in the organic nanopore network.

In addition to multiscale and multi-physics aspect of the problem, the geo-mechanics is another factor that needs to be considered. As described in Section 2, the geometrical differences between the organic capillaries and the crack could make them react to the applied stresses differently. The round shape of organic constituents allows

them to absorb stresses without much deformation compared to the crack which is slit shape.

The gas outflow from organic nanopore network to the crack influences the fluid pressure inside the crack and hence provides more resistance to the applied stresses. In that case the permeability of the crack could be maintained higher. Identification of this permeability enhancement is of significant practical interest since the source rock formations have limited permeability for the production. For this purpose, I consider a case where the multi-scale pore network depicted in Figure 17 is used to study the dynamics of the crack in the presence of the organic nanopore network. I am interested in monitoring the crack opening under various conditions of organic materials content ε_{kp} (O*rganic materials content is defined as the ratio of their pore volume to the total pore volume of the system*) and the nano-scale throat size distribution. The former reflects the natural gas storativity of the organic material while the latter controls the rate at which the gas is transported to the crack.

1. Fixed r_P and varying ε_{kp}

In this case, the organic material content is changed at a fixed throat size distribution (*i.e. percolation radius, and hence the absolute permeability of the organic material, is kept constant*). No flow condition is implemented on the boundaries except for the outlet of the crack where an outflow pressure value of 500 psi is assigned to deplete gas in the system. Even though pressure drop is relatively high for the size of my system,

Pore network properties	
R_P, nm	10
crack width, nm	120
c_{om}, psi^{-1}	6×10^{-6}
c_f, psi^{-1}	150×10^{-6}
ε_k	0.35, 0.8 and 0.98
Adsorption parameters & gas properties	
P_L, psi	1500
V_s, SCF/ton	100
D_k, nm^2/s	$f_1(r_p,T)$
D_s, nm^2/psi-s	5×10^{-12}
Viscosity, poise-s	$f_2(P,T)$
z	$f_3(P,T)$
Boundary and initial conditions	
P_i, psi	7000
P_{outlet}, psi	500
P_c, psi	15,000
Temperature, R	745

Table – 7: Design Parameters for organic materials interaction with crack at fixed r_P and variable ε_{kp}

the nano-scale time step would still allow us to keep monitoring the pressure changes within the system. The detailed design parameters are given in Table 7.

From Figure 18 one can observe that the crack width is influenced by the gas content of the organic nanoporous material. The gas outflow from the organic material supports the pressure inside the crack and keeps it open for a longer time.

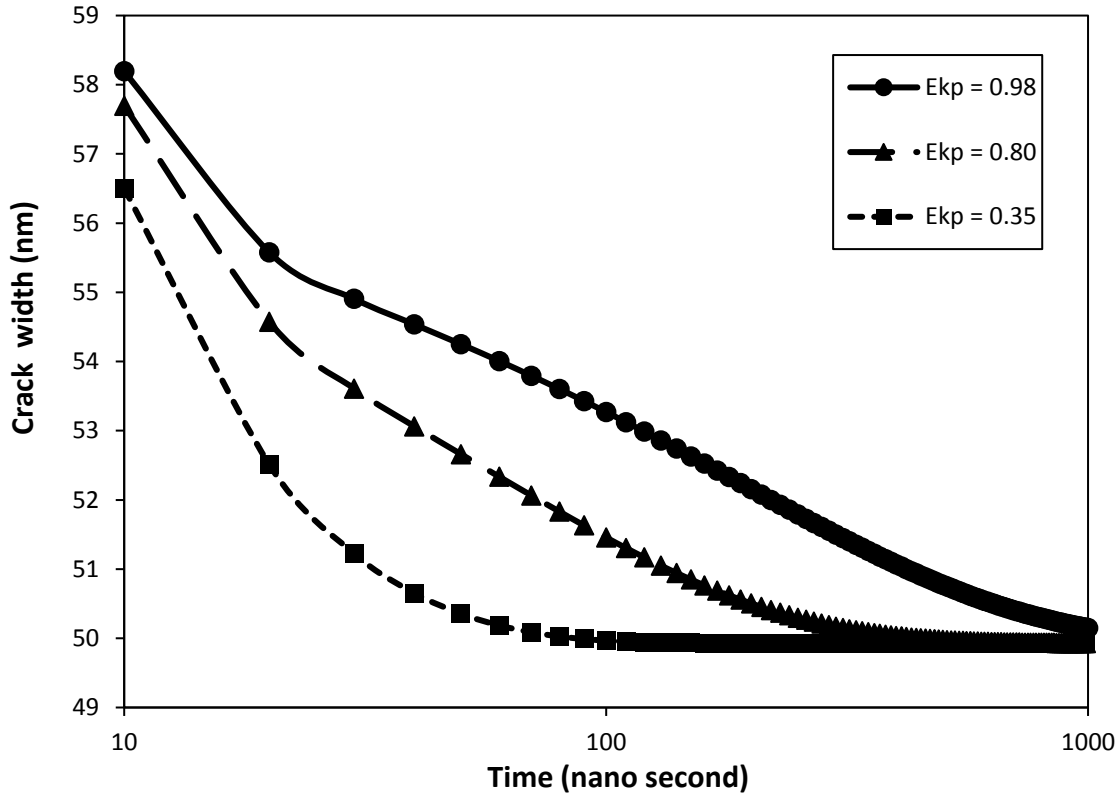

Figure 18 – Crack width change during depletion of the coupled organic material-crack system for different values of ε_{kp}

The degree by which the organic material supports the pressure in the crack is dependent on the amount of gas stored in the organic material, either as compressed gas or in the sorbed state, which is controlled by the size of the organic pores and the pressure.

2. Fixed ε_{kp} and variable r_P

Now, I investigate the effect of changing the percolation radius while the organic material content is kept constant. Changing the percolation radius would change the rate by which gas is transported from the organic nanopores to the crack.

Pore network properties	
R_P, nm	3, 6 and 10
crack width, nm	120
c_{om}, psi^{-1}	6×10^{-6}
c_f, psi^{-1}	150×10^{-6}
ε_k	0.98
Adsorption parameters & gas properties	
P_L, psi	1500
V_s, SCF/ton	100
D_k, nm^2/s	$f_1(r_p,T)$
D_s, nm^2/psi-s	5×10^{-12}
Viscosity, poise-s	$f_2(P,T)$
z	$f_3(P,T)$
Boundary and initial conditions	
P_i, psi	7000
P_{outlet}, psi	500
$P_{confining}$, psi	15,000
Temperature, R	745

Table – 8: Design Parameters for organic materials interaction with crack at fixed εkp and variable r_P

The same multi-scale pore network model parameters that were used in the previous part is used again but with a fixed organic content and a variable percolation radii.

The results is shown in Figure 19 and indicates that the dynamics of the crack width is also sensitive to the percolation radius of the organic material.

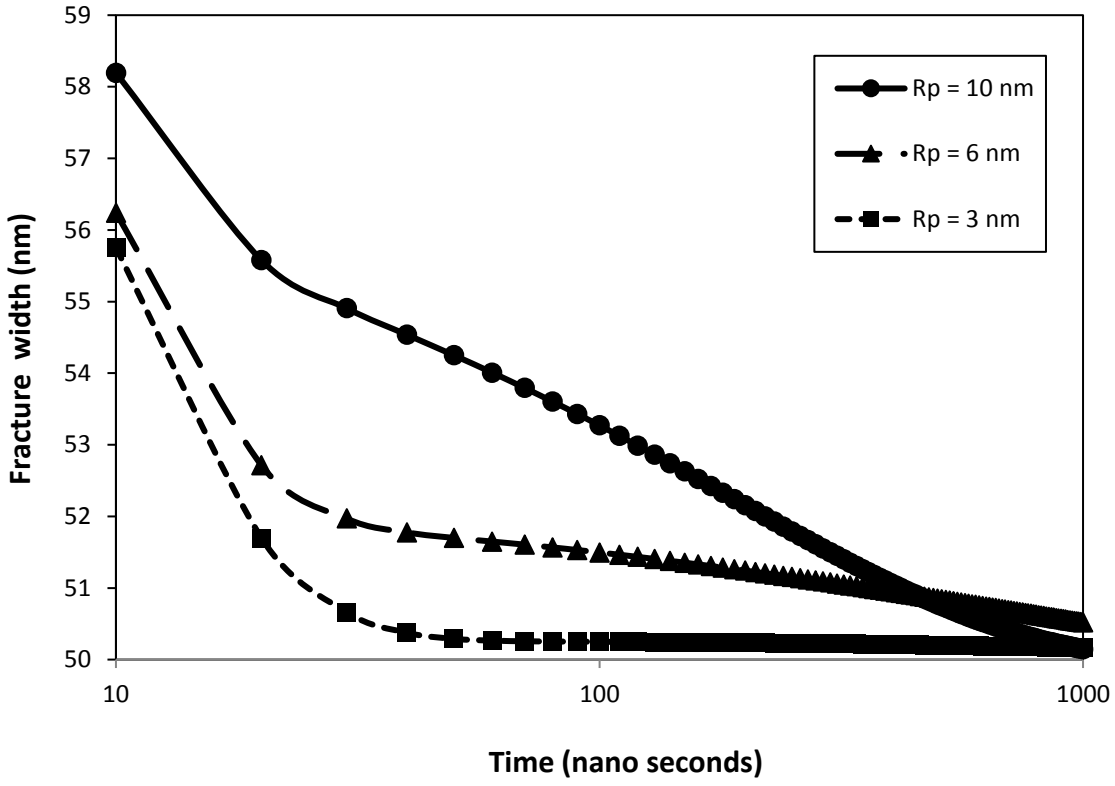

Figure 19 – Crack width change during the depletion of the coupled organic material-crack system for different values of r_p

In general, both the absolute permeability of the organic material and their gas content would change the dynamics of the crack permeability. Additionally, factors such as the pressure, adsorption parameters (*i.e. Langmuir pressure and volume*), and geo-mechanical properties of both media must be all taken into consideration to properly describe the organic pore network-crack interactions in the source rocks.

Gangi's permeability model could be useful in obtaining the dynamics of the micro-crack that is subjected to stress. Gangi's equation relates the micro-crack permeability to net stress as following:

$$k_f \sim w_f \sim \left(\frac{P_e}{P_1}\right)^m \qquad (28)$$

where, w_f is the width of the crack, P_1 and m are both related to the mechanical properties of the matrix with the crack, and P_e is the net stress.

The presence of the organic nanoporous material would affect the micro-crack dynamics and that can be significant as shown in the previous pages in Figures 18 and 19. Therefore, the net stress term P_e has to be corrected for the gas influx from the organic material.

I revisited the kerogen-inorganic matrix coupling model by Wasaki and Akkutlu (2015), where the apparent permeability of gas shale is derived assuming both the crack and the organic material are under the same pressure gradient (*i.e.* $\frac{\partial P}{\partial x}_{shale} = \frac{\partial P}{\partial x}_{kerogen} = \frac{\partial P}{\partial x}_{crack}$). With that assumption, the pressure in both the kerogen and the crack should be the same throughout the depletion of the shale reservoir which is inconsistent with our multi-scale pore network model observations where pressure gradient between the organic nanoporous material and the crack does exist and act as the driving mechanism of the viscous-diffusive-adsorptive kerogen gas influx (*i.e.* $Q_{kerogen} \sim k_{app,kerogen} \frac{\partial P}{\partial x}_{kerogen-inorganic\ crack}$).

3.3 Dual Continuum Approach for Transport Coupling

When dealing with different length scales in porous media, the direct simulation approach would be computationally expensive and time consuming. Alternatively, dual continuum approaches which are based on an approximation of fluid exchange between the two media of different length scales can be used. The basic idea is to relate the fluid exchange between the media to the pressure difference between them via some scaling factor known as the shape factor.

The dual porosity approximation for the fracture-matrix coupling was first introduced by Warren and Root (1963):

$$Q_{pss} = \sigma_{pss} k \left[(P_1) - (P_2) \right] \tag{29}$$

where, σ_{pss} is the shape factor, k is the permeability of the medium 1. Implementing this equation in reservoir simulations improved the computational time significantly. However, one of its limitations is its lack of accuracy in predicting the fluid exchange rate during the early time of production. Some effort has been done to correct for the transient effect such as the work of Zimmerman et al. (1993), where the flow exchange rate in the early time can be approximated by solving for Vermeulen series using Crank's sphere diffusion model. The final dual porosity equation in Zimmerman's model was given as:

$$Q = \sigma_{pss} k \frac{[P_1 - P_i\,]^2 - [P_2 - P_i\,]^2}{2[P_1 - P_i\,]} \tag{30}$$

where, P_i is the initial pressure in both media. It can be shown that the above formula would reduce to the original Warren and Root equation at later time.

In my case of organic material-crack duality, however, equations 29 and 30 cannot be directly applied. Firstly, the gas is a highly compressible fluid and its state would be dependent on the pressure which varies significantly between the two media. Additionally, the multi-physics gas transport in the organic materials is pressure-dependent. In order to account for these two effects, the fluid pressure of the organic material-crack system is subjected to the following transformation:

$$\psi(P) = \frac{1}{2}\int \frac{\left(R^* + a + \frac{\mathrm{b}}{\mathrm{P}}\right) P}{\mu Z} dP \qquad (31)$$

where, ψ is the newly-defined pressure function, whichis similar to the definition of the well-known pseudo-pressure functionused in natural gas engineering to account for changes in gas compressibility and viscosity but now including the pressure-dependent parameters of the organic material including its apparent permeability.

Now, similar to Zimmerman et al. (1993) work, the fluid exchange between the organic material and the associated crack has the following form:

$$Q = \sigma_{pss} k \frac{[\psi(P_{om}) - \psi(P_i)\,]^2 - [\psi(P_f) - \psi(P_i)\,]^2}{2[\psi(P_{om}) - \psi(P_i)\,]} \qquad (32)$$

The detailed derivation and validation of equation 32 is presented in Appendix B. In the equation, k is the absolute permeability of the organic materials, P_1, P_2, and P_i are the organic, the crack, and the initial pressures, respectively.

The pseudo-steady state coupling term can now be given as:

$$Q_{pss} = \sigma_{pss} k\,[\psi(P_{om}) - \psi(P_f)] \qquad (33)$$

The transient effect can be written based on the ratio of fluid exchange terms as:

$$f_T = \frac{Q_{pss}}{Q} \tag{34}$$

where, f_T is the transient factor for the coupling term, which, using equations 33 and 34, is related to the pseudo-pressure function as follows:

$$f_T = \frac{[\psi(P_{om}) - \psi(P_i)\,]^2 - [\psi(P_f) - \psi(P_i)\,]^2}{2[\psi(P_{om}) - \psi(P_i)\,][\psi(P_{om}) - \psi(P_f)]} \tag{35}$$

Then, the coupling term is given as:

$$Q = \sigma_{pss} k\, f_T [\psi(P_{om}) - \psi(P_f)] \tag{36}$$

Now, I can use the multi-scale pore network model coupled with crack to study the behavior of f_T. The exchange flow rate in the organic material-crack system along with the pressure values in both media can be obtained from our multi-scale pore network model. Hence, f_T can be computed using equation 35.

f_T is bounded between upper and lower limits. The lower limit is when sufficient time is reached so the flow is at pseudo-steady state and its value is close to 1. In this case, the Warren and Root equation with pseudo-pressure function can be used to describe the coupling between organic materials and cracks. On the other hand, the transient factor was found to be greater than 2 at the early time indicating the significance of accounting for the transient effect. Using the parameter values given in Table 9, these are shown in Figure 20.

Pore network properties	
R_P, nm	6
crack width, nm	120
c_{om}, psi^{-1}	6×10^{-6}
c_f, psi^{-1}	150×10^{-6}
ε_k	0.7
Adsorption parameters & gas properties	
P_L, psi	1500
V_s, SCF/ton	100
D_k, nm^2/s	$f_1(r_p,T)$
D_s, nm^2/psi-s	5×10^{-12}
Viscosity, poise-s	$f_2(P,T)$
z	$f_3(P,T)$
Boundary and initial conditions	
P_i, psi	7000
$P_{outlet-}$, psi	500
P_c, psi	15,000
Temperature, R	745

Table – 9: Parameters used in the case study for f_T.

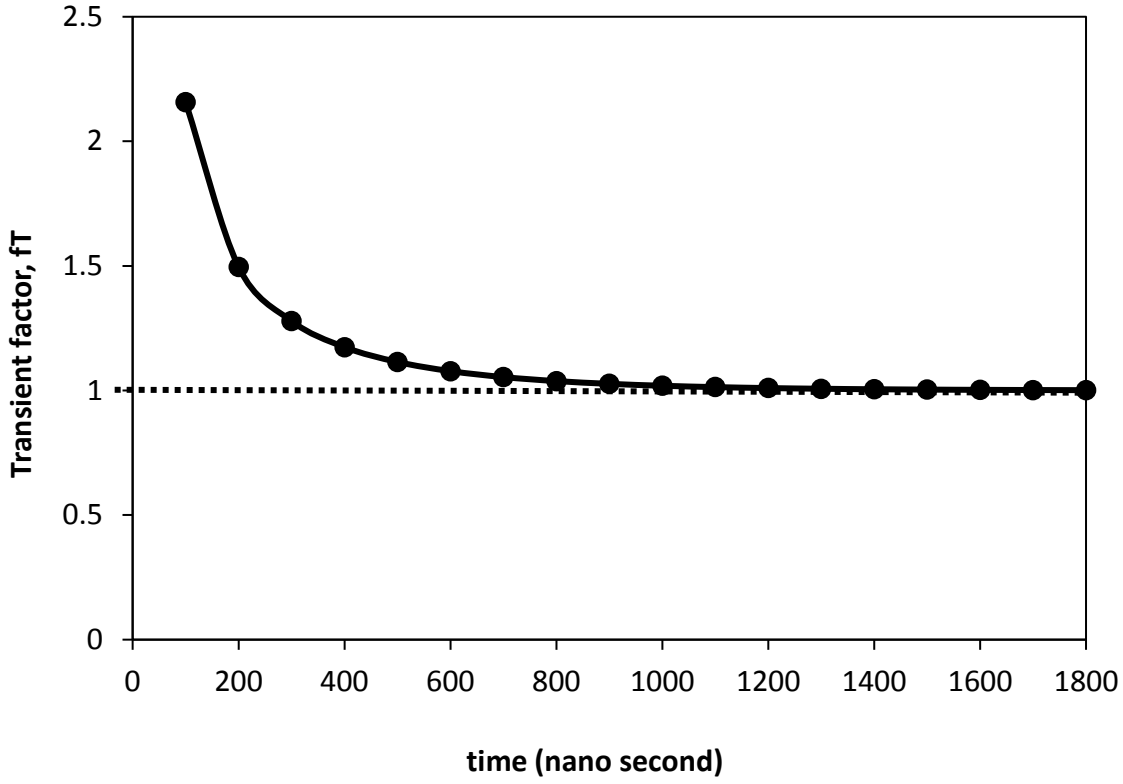

Figure 20 – f_T calculated using the data obtained from the multiscale pore network model

In Figure 21, it can be seen that the ratio of gas exchange rate to the pressure difference at the matrix-crack interface yields a constant response during the transient and pseudo-steady state regimes when f_T is included (*i.e. the constant response here represents the shape factor multiplied by the absolute permeability*) while the original Warren and Root deviates at the early time.

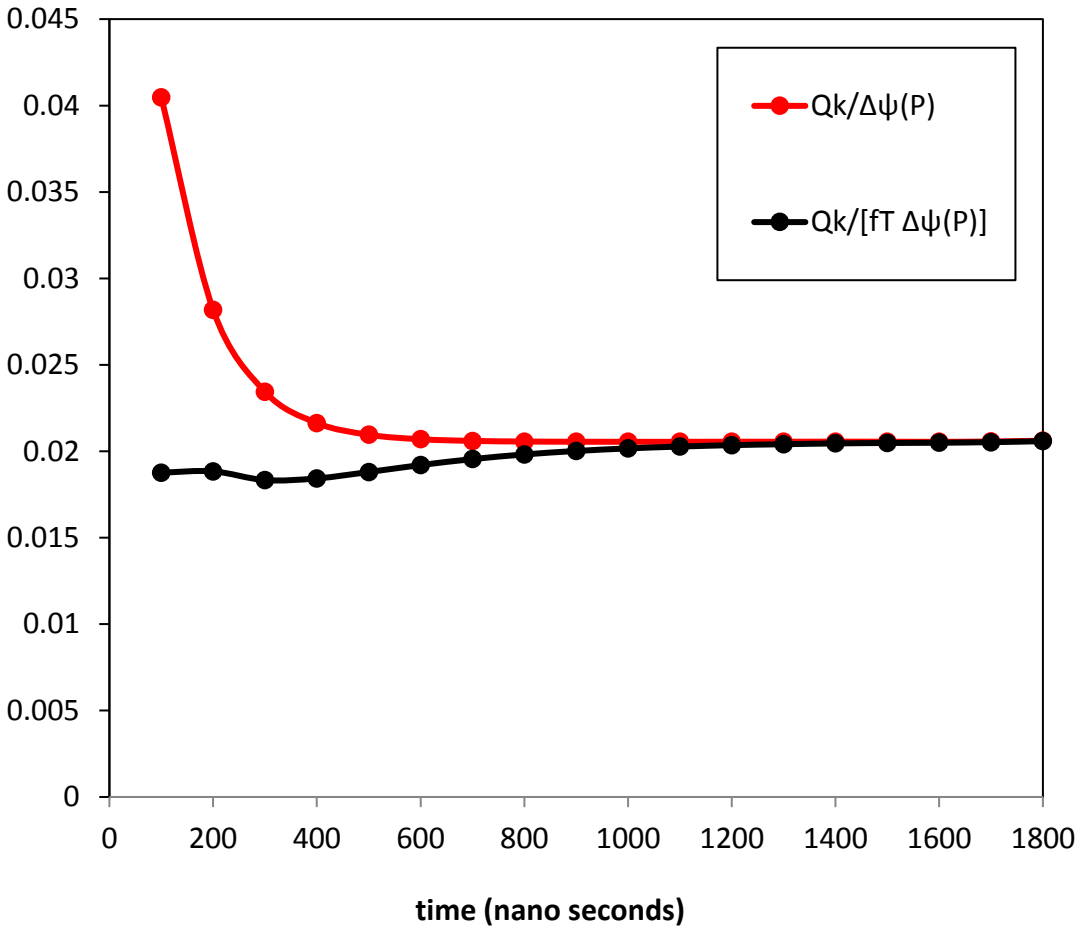

Figure 21 – Flow rate between organic materials and crack to the pressure difference between them using the Warren and Root equation and its modified version where f_T is included. Note: the modified version yields a constant response while the original one deviates at the early time.

3.4 Dual Continuum Modeling of Organic Materials-Crack System

At the continuum scale, the organic and inorganic heterogeneities are represented by some volume averaged quantities such as the organic materials content. That is done because it would not be feasible or computationally possible to include all the nano-scale details when making the simulations at the reservoir scale. The organic material-crack flow exchange term derived in the previous section can serve as the link between the nano-scale and the reservoir scale.

At the continuum level, the gas mass balance in the cracks is given as follows:

$$\frac{\partial\left(\rho_g \emptyset_f \left(1-\varepsilon_{kp}\right)\right)}{\partial t} = \nabla\left(\rho_g \frac{k_f}{\mu}\nabla P\right) - Q \tag{37}$$

where, ε_{kp} is the organic materials contents, k_f is the permeability of the crack, $\emptyset_f$ is the porosity of the crack, p_g is the gas density, and μ is the gas viscosity. Q is the coupling term.

The permeability and porosity of the crack is pressure-sensitive and as explained previously, the mechanical properties are determined at the effective stress which is also influenced by the gas influx from the organic material. Therefore, the volume (or porosity) and permeability of the crack should be updated with the effective crack pressure value at each time step.

Similarly, the continuity equation around the organic material can be written as:

$$\frac{\partial\left(\rho_g \emptyset\left(\varepsilon_{kp}-\varepsilon_{ks}\right)\right)}{\partial t} = Q \tag{38}$$

where, ε_{ks} is the fraction of the pore volume taken by the sorbed gas in the organic nanopores.

Then, equations 37 and 38 are solved simultaneously for the pressure distribution of the system. All of parameters in these equations are pressure-dependent and should be updated at each time step to properly describe the dynamics of the system.

Now, a simplified case is considered where multiple cracks hydraulically-interacting with some organic materials scattered around them as shown in Figure 22. There are two approaches that can be followed in describing the dynamics of this system. We may consider each medium as a separate grid block and write the mass balance for it.

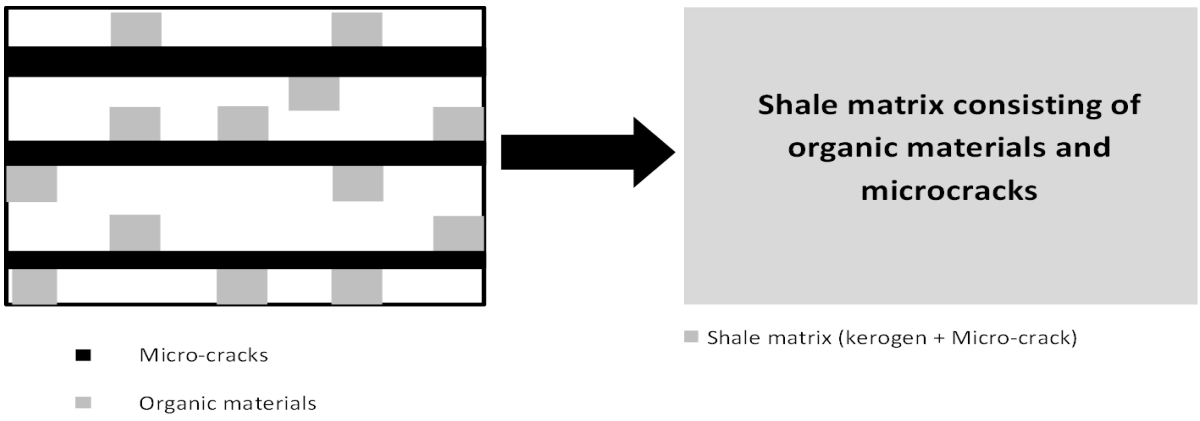

Figure 22 – Left: A representation of the shale matrix where organic material and cracks are distributed separately. Right: Shale matrix is considered as a whole where the flow exchange between the organic materials and the cracks within the matrix is captured by the coupling term $Q_{organic}$ and ε_{kp}.

Rock properties	
k_{om}, µD	0.5
k_f, µD	5
c_{om}, psi^{-1}	6×10^{-6}
c_f, psi^{-1}	150×10^{-6}
$\emptyset_{om}$	0.05
$\emptyset_f$	0.1
Adsorption parameters & Gas properties	
P_L, psi	1500
V_s, SCF/ton	100
D_k, nm^2/s	$f_1(r_p,T)$
Ds, nm^2/psi-s	5×10^{-12}
Viscosity, poise-s	$f_2(P,T)$
z	$f_3(P,T)$
Dimensions	
Bulk volume, μm^3	150
Boundary and initial conditions	
P_i, psi	3500
P_{outlet}, psi	500
P_c, psi	15,000
Temperature, R	745

Table – 10: Design parameters for the dual-porosity continuum modeling case study

Alternatively, we can follow the continuum approximation given by equations 37 and 38. The two approaches are followed for the sake of comparison. We can think of the first one as the exact solution to the problem and the second one as some approximation because it involves some assumptions as explained previously.

The design parameters for this example are given in Table 9. The total flow rate out of the whole system would be the basis of comparison between the two cases. In both

approaches, the permeability and the porosity of the cracks are updated at each step using Gangi's model.

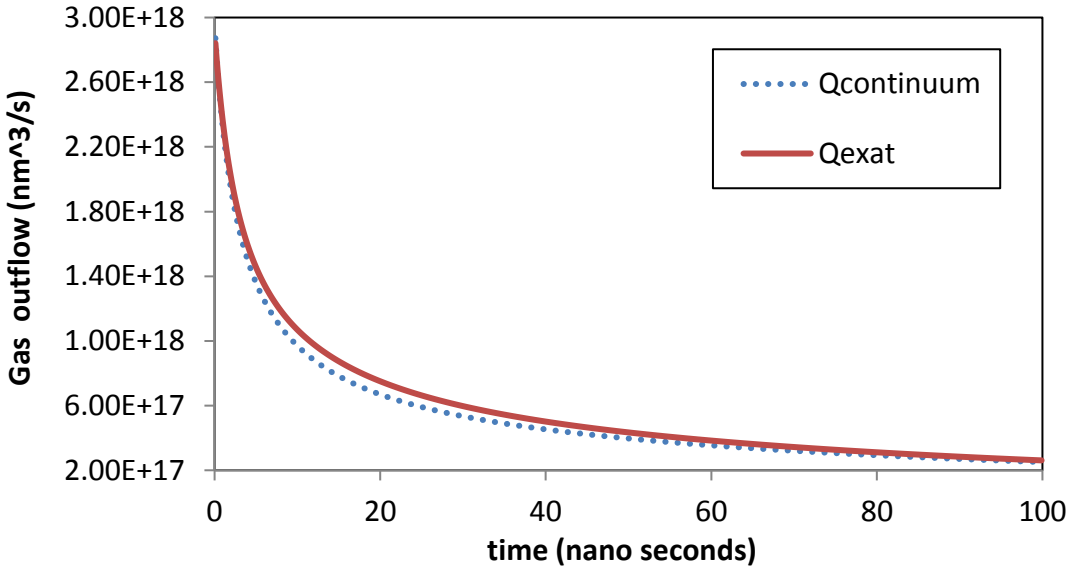

Figure 23 – Total flow rate out of the dual porosity matrix with organic materials and micro-cracks as a function of time using the exact (*i.e. subgrid blocks*) and the continuum approximation.

The results shown in Figure 23 indicate that the flow rate of the continuum approximation matches the exact solution reasonably at both the early time, when most of the gas is produced from the cracks only, as well as in the later time, when the gas in the organic material starts contributing to the gas release.

4. FIELD SCALE SIMULATION OF GAS FLOW AND PRODUCTION*

In this section, the role of the organic material-crack coupling on the overall production is investigated at the reservoir scale using the continuum approach presented in Section 3. The conceptual model is illustrated in Figure 24 where a single hydraulic fracture in a gas shale formation is considered. The total porosity of the system is fixed at 5% and then, organic materials are introduced by increasing their fraction ε_{kp} from zero to 0.6 while maintaining the total porosity the same. The shale matrix is subdivided into grid blocks. At each grid block, the nonlinear equations 37 and 38 are solved simultaneously using Newton-Raphson method.

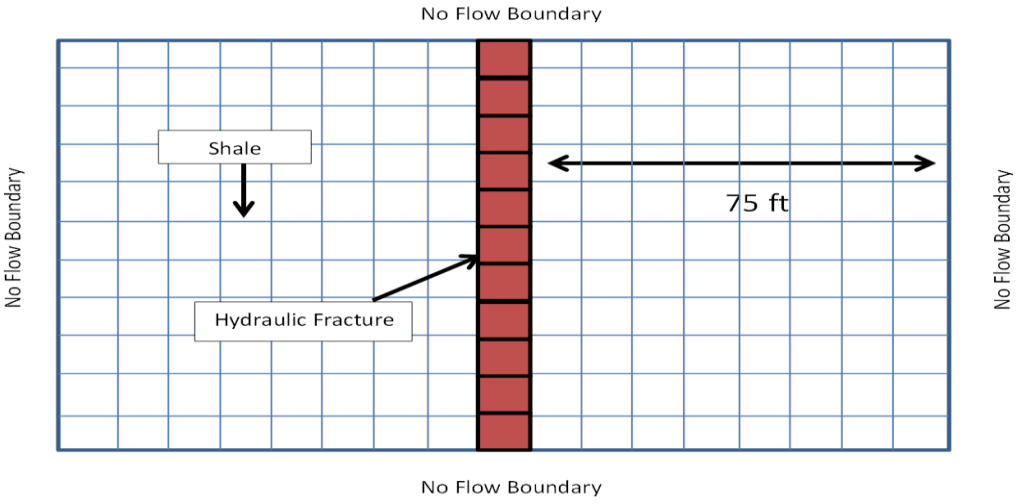

Figure 24 – Conceptual model built for the field scale simulation of shale matrix

* Reprinted with permission from "Matrix-Fracture Interactions during Flow in Organic Nanoporous Materials under Loading" by Alafnan & Akkutlu, 2017. Journal of Transport in Porous Media.

Rock properties	
k_{om}, µD	7.5 x 10^{-2}
k_f, µD	10
c_{om}, psi^{-1}	6 x 10^{-6}
c_f, psi^{-1}	150 x 10^{-6}
Total porosity	5%
ε_{kp}	0, 0.33, and 0.6
Adsorption parameters & gas properties	
P_L, psi	1500
V_s, SCF/ton	100
D_k, nm^2/s	$f_1(r_p,T)$
D_s, nm^2/psi-s	5 x 10^{-12}
µ, poise-s	$f_2(P,T)$
z	$f_3(P,T)$
Reservoir dimensions	
Width, ft	150
HF height, ft	15
HF length, ft	30
Boundary and initial conditions	
P_i	3500
P_{HF}	500
P_c	15,000
Temperature, R	745

Table – 11: Field scale simulation parameters.

No flow boundary conditions are assumed at the edges and constant outflow pressure in the hydraulic fracture is assigned to deplete the reservoir. Then, the overall gas influx to the hydraulic fracture is calculated.

Note that, at each time step, the crack permeability is updated for the presence of effective stress using Gangi's model:

$$k_f = k_{f,o}\left[1 - \left(\frac{P_c - \alpha P}{P_1}\right)^m\right]^3 \quad (39)$$

where, $k_{f,o}$ is the crack permeability at zero stress, P_c is the confining pressure, α *the Biot coefficient*, P_1 and m are the Gangi's model parameters. In this case and similar to the values used in (Wasaki and Akkutlu, 2015) are m and α are 0.5, respectively, while P_1 is 26,000 psi.

In Figure 25 one observes that considering the duality of the shale matrix influences the overall production. The production was highest when ε_{kp} is zero. In that case, the gas molecules pathway to the hydraulic fracture is not associated with the organic

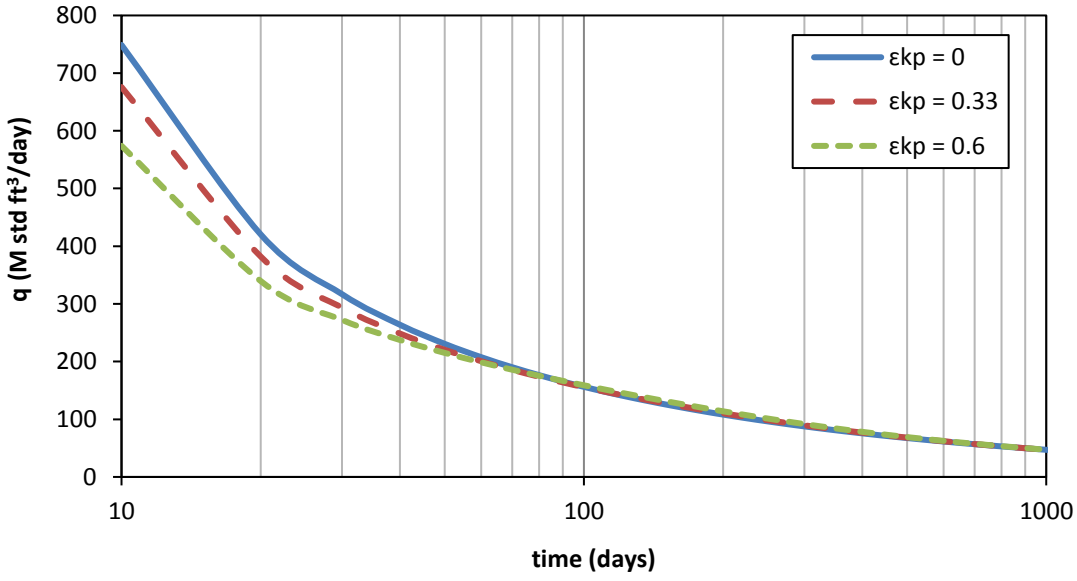

Figure – 25 Gas release from the shale formation to the hydraulic fracture

nanopores, nor its sorption and nano-scale confinement effects. These additional transport complexities add more resistance to the overall shale gas productivity which can be seen in the other two cases where portion of the gas is stored in the organic material (*i.e. when* ε_{kp} *is 0.33 and 0.6*).

To check for role of the non-Darcian transport mechanisms at the field scale, I considered a case where ε_{kp} is 0.7 and repeat the simulation with and without the non-Darcian transport mechanisms (*i.e. the transport in the organic materials is viscous only*). The results presented in Figure 26 shows that the overall production is underestimated by 10-20% if the non-Darcian mechanisms are excluded.

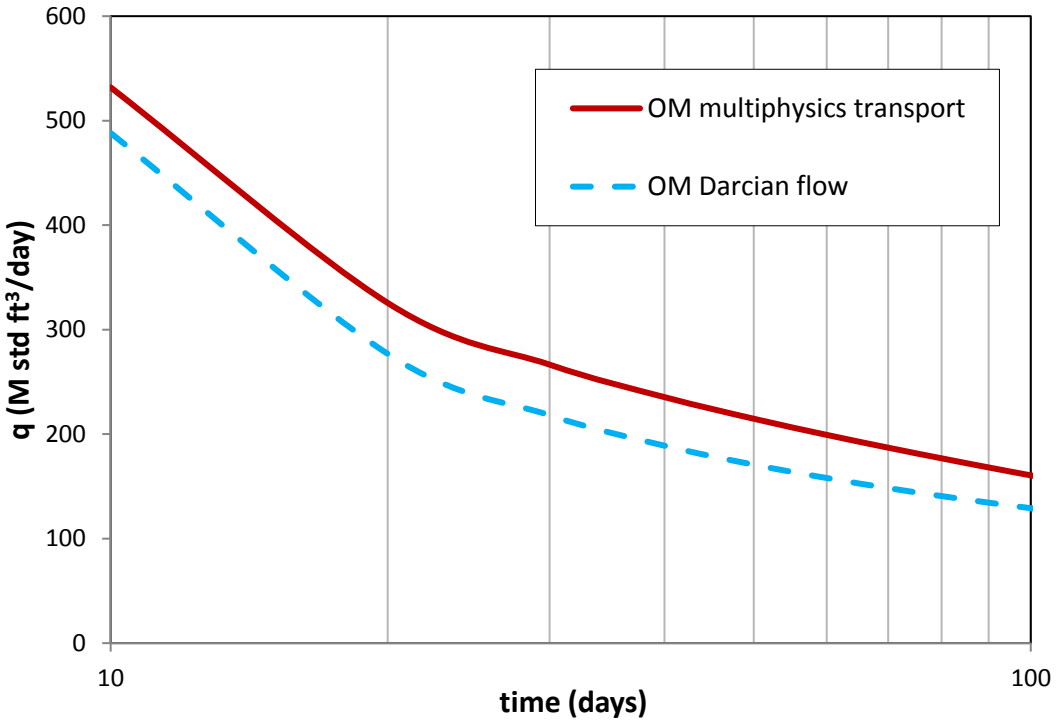

Figure – 26 Multi-physics transport of the organic materials at the field scale.

The previous example illustrates the importance of properly characterizing the source rock and quantifying the portion of organic material within the matrix and then, modeling the gas transport in these organic pockets considering the advective-diffusive-adsorptive mechanisms coupled with the gas flow in cracks.

5. SUMMARY AND FUTURE WORK

5.1 Summary

In this dissertation, the local nano-scale heterogeneity associated with the presence of organic material is upscaled to the continuum scale of shale matrix. Firstly, I started by considering the transport in single nano-capillary equation of the organic material and I discussed how the physics of the transport deviates from the simple Stoke's flow due to the degree of confinement and the fluid-solid interactions. Then, the concept of pore network modeling was used to study the transport at a larger scale, i.e., the scale of the organic nanopore network. I used the percolation theory to derive some upscaled coefficients for the different mechanisms that coexist in the transport of gas. Next, a multi-scale pore network model was built to simulate the natural gas flow between organic material and crack. Based on the results and using the dual porosity approach, a coupling term is defined for predicting the flow exchange between organic material and the crack. That coupling term was also used in a large scale reservoir simulator to study the dynamics of the shale matrix. The steps involved in this work are summarized in Figure 27:

- The physics of the fluid transport in the nano-scale single organic materials capillary were studied.
- The local nano-scale capillary equation was upscaled via pore network modeling approach.
- The representative elementary volume of the organic materials is defined

using the pore network model.

- Sensitivity analysis on the organic materials apparent permeability was carried out. It was found that the apparent permeability was most influenced by the pressure and the effective throat size.
- Percolation theory and pore network modeling were used to derive a formula for the organic materials apparent permeability.
- Flow regimes within the organic materials were studied. It was found that viscous, diffusive, and adsorptive mechanisms coexist. Péclet and Biot numbers were used to characterize the mode of the transport.
- Then, a multiscale pore network model was built to study the duality of the organic materials-crack system. It was found that the presence of the organic materials influences the dynamics of the cracks.
- Dual continuum approach very similar to Warren and Root was used to couple the transport in the organic materials-crack system with some modifications for the dependency of the transport on the pressure.

5.2 Future Work

The work presented in this dissertation links the microscopic transport at nano-scale to reservoir-scale via pore network modeling. In petroleum engineering, we deal with some volume averaged quantities such as permeability and porosity. Our goal was to redefine these transport coefficients to account for the viscous flow, diffusion, and adsorption mechanisms in the organic materials of gas shale.

In the future, 3-D imaging techniques can be used in building the pore network model along with the pore and throat size distributions to build a pore network model that reflects real case scenarios honoring the local heterogeneities of the organic materials. Such models can then be linked with percolation theory to obtain the flow coefficients of the organic materials apparent permeability.

Additionally, the organic materials-crack coupling term that was derived in this work needs to be linked with the other aspects of the shale reservoirs such as the inorganic matrix, hydraulic, and natural fractures to investigate the role of organic material on the overall shale gas well production.

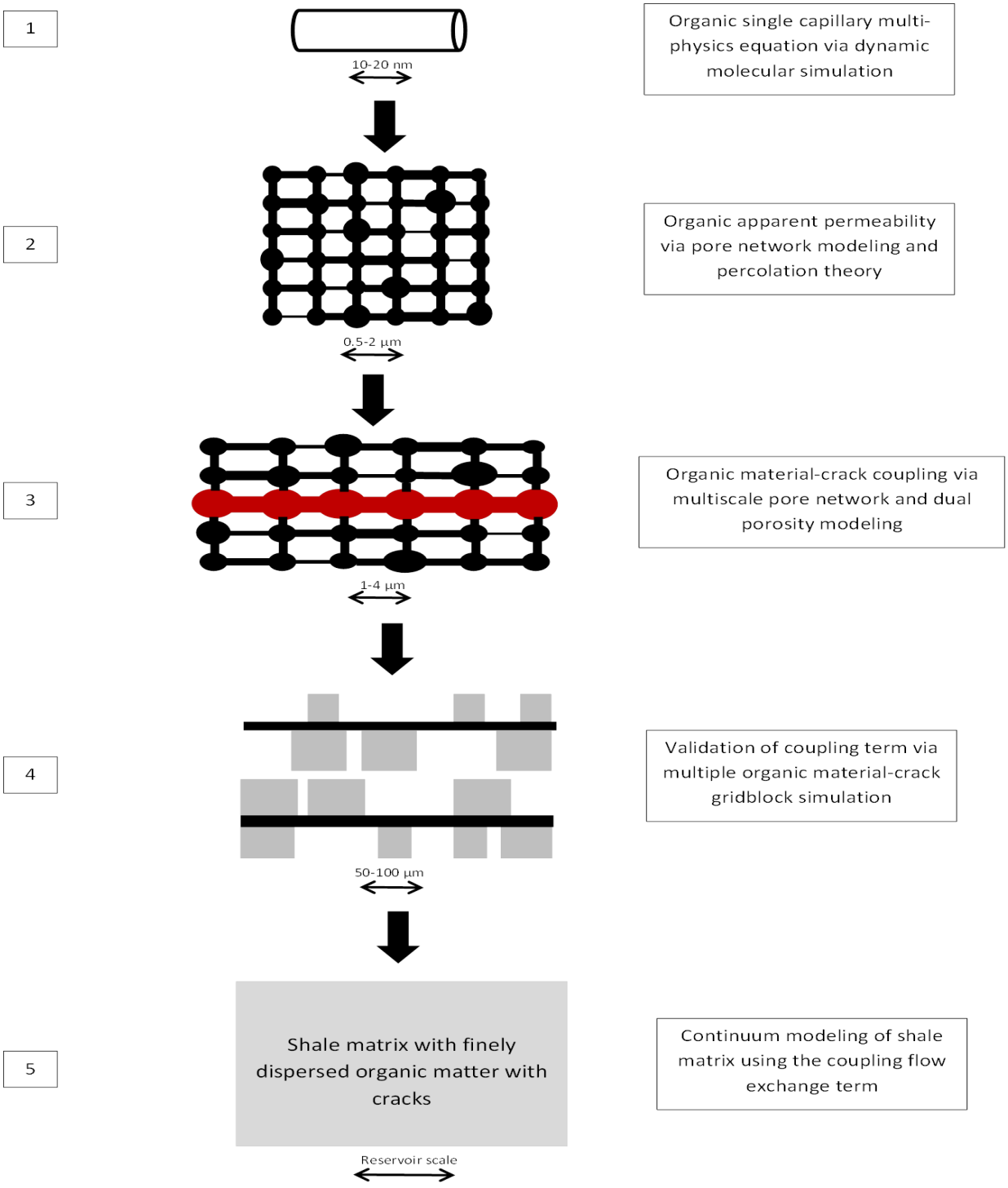

Figure 27 – An outline of the steps followed in this dissertation to describe the shale matrix dynamics

REFERENCES

Ambrose, R.J., Hartman, R.C., Diaz-Campos, M., Akkutlu, I.Y., Sondergeld, C.H., 2012, "Shale Gas-in-Place Calculations Part I: New Pore-Scale Considerations", SPE Journal. 17, 219–229.

Blunt, M., King, M.J., Scher, H., 1992, "Simulation and theory of two-phase flow in porous media", Physical Review A. 46, 7680–7699.

Celia, M.A., Reeves, P.C., Ferrand, L.A., 1995, "Recent advances in pore scale models for multiphase flow in porous media", Reviews of Geophysics. 33, 1049–1057.

Ertekin, T., King, G.A., Schwerer, F.C., "Dynamic Gas Slippage: A Unique Dual-Mechanism Approach to the Flow of Gas in Tight Formations", SPE Formation Evaluation. 1, 43–52.

Fathi, E., Akkutlu, I.Y., 2011, "Mass Transport of Adsorbed-Phase in Stochastic Porous Medium with Fluctuating Porosity Field and Nonlinear Gas Adsorption Kinetics", Transport in Porous Media. 91, 5–33.

Fathi, E., Tinni, A., Akkutlu, I.Y., 2012, "Shale Gas Correction to Klinkenberg Slip Theory", SPE Americas Unconventional Resources Conference.

Gangi, A.F., 1978, “Variation of whole and fractured porous rock permeability with confining pressure”, International Journal of Rock Mechanics and Mining Sciences & Geomechanics Abstracts. 15, 249–257.

Guo, C., Xu, J., Wu, K., Wei, M., Liu, S., 2015, “Study on gas flow through nano pores of shale gas reservoirs”, Fuel. 143, 107–117.

Hou, Y., He, S., Wang, J., Harris, N.B., Cheng, C., Li, Y., Pedersen, P., 2015, “Preliminary study on the pore characterization of lacustrine shale reservoirs using low pressure nitrogen adsorption and field emission scanning electron microscopy methods: a case study of the Upper Jurassic Emuerhe Formation, Mohe basin, northeastern China”, Canadian Journal of Earth Sciences. 52, 294–306.

Hsieh, T.-H., Huang, Y.-S., Shen, M.-Y., 2015, “Mechanical properties and toughness of carbon aerogel/epoxy polymer composites”, Journal of Materials Science. 50, 3258–3266.

Javadpour, F., 2009, “Nanopores and Apparent Permeability of Gas Flow in Mudrocks (Shales and Siltstone)”, Journal of Canadian Petroleum Technology. 48, 16–21.

Joekar-Niasar, V., Hassanizadeh, S.M., 2012, “Analysis of Fundamentals of Two-Phase Flow in Porous Media Using Dynamic Pore-Network Models: A Review. Critical Reviews in Environmental Science and Technology”, 42, 1895–1976.

Kang, S.M., Fathi, E., Ambrose, R.J., Akkutlu, I.Y., Sigal, R.F., 2011, “Carbon Dioxide Storage Capacity of Organic-Rich Shales”, SPE Journal. 16, 842–855.

Kou, R., Alafnan, S.F.K., Akkutlu, I.Y., 2016 “Multi-scale Analysis of Gas Transport Mechanisms in Kerogen”, Transport in Porous Media. 116, 493–519.

Kwon, O., Kronenberg, A.K., Gangi, A.F., Johnson, B., Herbert, B.E., 2004, “Permeability of illite-bearing shale: 1. Anisotropy and effects of clay content and loading. Journal of Geophysical Research: Solid Earth”, 109.

Mavko, G.M., Nur, A., 1978, “The effect of nonelliptical cracks on the compressibility of rocks”, Journal of Geophysical Research. 83, 4459.

Mehmani, A., Prodanović, M., Javadpour, F., 2013, “Multiscale, Multiphysics Network Modeling of Shale Matrix Gas Flows”, Transport in Porous Media. 99, 377–390.

O'Carroll, C., Sorbie, K.S., 1993, "Generalization of the Poiseuille law for one- and two phase flow in a random capillary network", Physical Review E. 47, 3467–3476.

Riewchotisakul, S. and Akkutlu, I.Y., 2015, "Adsorption–enhanced Transport of Hydrocarbons in Nanometer-scale Organic Pores", SPE-175107, paper presented during the SPE Annual Technical Conference and Exhibition in Houston.

Sakhaee-Pour, A. Bryant, S., 2012, "Gas Permeability of Shale", SPE Reservoir Evaluation & Engineering 15 (04): 401–409.. . doi:10.2118/146944-PA.

Sarkisov, L., Monson, P.A., 2001 "Modeling of Adsorption and Desorption in Pores of Simple Geometry Using Molecular Dynamics", Langmuir. 17, 7600–7604.

Singh, H., Javadpour, F., Ettehadtavakkol, A., Darabi, H., 2014, "Nonempirical Apparent Permeability of Shale", SPE Reservoir Evaluation & Engineering. 17, 414–424.

Wang, F.P. and Reed, R.M., 2009, "Pore Networks and Fluid Flow in Gas Shales", Paper SPE 124253 presented at the SPE Annual technical Conference and Exhibition.

Wasaki, A. and Akkutlu, I.Y., 2015, “Permeability of Organic-rich Shale”, SPE Journal, Volume 20 (6), 1384-1396.

Wasaki, A., Akkutlu, I.Y., 2015, “Dynamics of Fracture-matrix Coupling during Shale Gas Production: Pore Compressibility and Molecular Transport Effects”, SPE Annual Technical Conference and Exhibition.

Zhang, R., Ning, Z., Yang, F., Wang, X., Zhao, H., Wang, Q., 2015, “Impacts of nanopore structure and elastic properties on stress-dependent permeability of gas shales”, Journal of Natural Gas Science and Engineering. 26, 1663–1672.

Zhou, S., Yan, G., Xue, H., Guo, W., Li, X., 2016, “2D and 3D nanopore characterization of gas shale in Longmaxi formation based on FIB-SEM”, Marine and Petroleum Geology. 73, 174–180.

Zimmerman, R.W., Chen, G., Hadgu, T., Bodvarsson, G.S., 1993, “A numerical dual-porosity model with semianalytical treatment of fracture/matrix flow”, Water Resources Research. 29, 2127–2137.

APPENDIX A*

DISCRETIZATION OF THE MASS BALANCE IN THE PORE-NETWORK MODEL

The calculations around each node (pore) are carried out by the material balance equation given in equation 1. Then, the discretized form is illustrated by taking a single pore interconnected with two throats as shown in Figure 27.

To avoid complexity, the fluid velocity in the discretized form is taken as the Hagen-Poiseuille velocity. The same procedure can be done with the modified Hagen-Poiseuille form.

$$A_{in}\,(u\rho)_{in} - A_{out}\,(u\rho)_{out} + \frac{\partial(\rho V^*)_{pore}}{\partial t} = 0 \tag{40}$$

$$\rho = \frac{PM}{zRT} \tag{41}$$

$$u = \frac{R^2}{8\mu}\frac{\partial P}{\partial x} \tag{42}$$

$$A = \pi R^2 \tag{43}$$

* Reprinted with permission from "Matrix-Fracture Interactions during Flow in Organic Nanoporous Materials under Loading" by Saad Alafnan & Yucel Akkutlu, 2017. Journal of Transport in Porous Media.

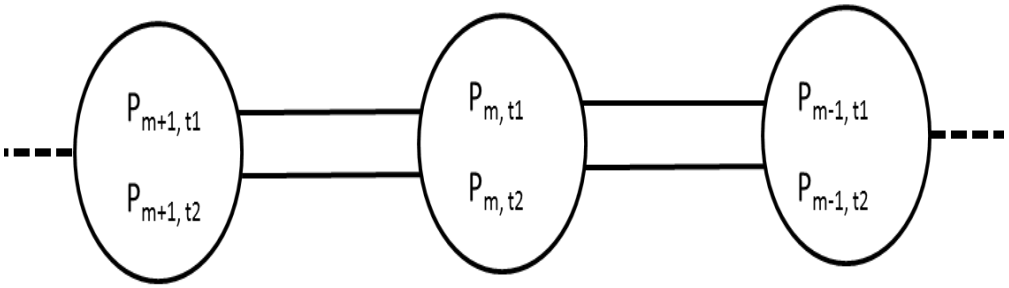

Figure 28 — Schematic of single pore interconnected with two throats to explain how the material balance is discretized for the pore network model.

Then, the mass flux is:

$$u\rho = \frac{MR^2}{8RT}\left(\frac{P}{\mu z}\right)\frac{\partial P}{\partial x} = \frac{MR^2}{16RT(\mu z)_{avg}}\frac{P_1^2 - P_2^2}{L} \qquad (44)$$

Mass Accumulation:

$$\frac{\partial(\rho V)_{pore}}{\partial t} = \frac{\frac{M}{RT}\left[\left(\frac{PV^*}{z}\right)_{t1} - \left(\frac{PV^*}{z}\right)_{t2}\right]}{\Delta t} \qquad (45)$$

Continuity equation becomes:

$$\frac{M\pi {R_{in}}^4}{16RT(\mu z)_{avg,\,in}}\frac{P_{in}^2 - P_{pore}^2}{L} - \frac{M\pi {R_{out}}^4}{16RT(\mu z)_{avg,out}}\frac{P_{pore}^2 - P_{out}^2}{L} \qquad (46)$$

$$+\frac{M}{RT}\frac{\left[\left(\frac{P_{pore}V^*}{z}\right)_{t1} - \left(\frac{P_{pore}V^*}{z}\right)_{t2}\right]}{\Delta t} = 0$$

where, V^* is the pore volume corrected for the presence of the adsorbed layer

using Langmuir adsorption model:

$$V^* = V\left(1 - \frac{V_s}{V}\right), \qquad V_s = V_{sL}\frac{P}{P_L + P} \tag{47}$$

Rearrangement and simplification of the equation:

$$\left[\frac{\pi {R_{out}}^4}{16L(\mu z)_{avg,out}} + \frac{\pi {R_{in}}^4}{16L(\mu z)_{avg,\,in}}\right] {P^2_{pore}}_{t2} + \frac{1}{\Delta t}\left(\frac{P_{pore}V^*}{z}\right)_{t2} \tag{48}$$

$$= \frac{\pi {R_{in}}^4}{16L(\mu z)_{avg,\,in}} P^2_{in} + \frac{\pi {R_{out}}^4}{16L(\mu z)_{avg,out}} P^2_{out} + \frac{1}{\Delta t}\left(\frac{P_{pore}V^*}{z}\right)_{t1}$$

System of nonlinear equations is to be solved for pressure at each pore as a function of time step Δt.

$$aP_m{}^2 + \mathrm{b}P_m + cP_S{}^2 + dP_N{}^2 + eP_{NE}{}^2 + fP_{NW}{}^2 + gP_{SE}{}^2 + hP_{SW}{}^2 + iP_{UN}{}^2 \tag{49}$$
$$+ jP_{DS}{}^2 + kP_{UNE}{}^2 + lP_{UNW}{}^2 + \cdots + c1 = 0$$

a, b, c, d, e … are all function of pressure and that nonlinear system of equations can be solved using the iterative Newton-Raphson method:

$$P_{n,t+1} = P_{n,t} + \frac{f\left(P_{n,t}\right)}{f'\left(P_{n,t}\right)} \tag{50}$$

For the multiscale network, the velocity in the crack is given by equation (16).

APPENDIX B[*]

THE USE OF CRANK SPHERE MODEL IN DEFINING THE TRANSIENT FACTOR

On our case the Crank sphere model cannot be used directly as given in Zimmerman et al. (1993) because of the pressure dependence of the organic material permeability.

$$\frac{P_{om} - P_i}{P_f - P_i} = [1 - exp(-Ckt)]^{1/2} \qquad (51)$$

One way to linearize the problem is to replace the pressure with a pressure function. In this case the permeability *k* would be the intrinsic or liquid permeability.

$$\frac{\psi(P_{om}) - \psi(P_i)}{\psi(P_f) - \psi(P_i)} = [1 - exp(-Ckt)]^{1/2} \qquad (52)$$

Rearrangement:

$$\left(1 - \left(\frac{\psi(P_{om}) - \psi(P_i)}{\psi(P_f) - \psi(P_i)}\right)\right)^2 = \exp(-Ckt) \qquad (53)$$

[*] Reprinted with permission from "Matrix-Fracture Interactions during Flow in Organic Nanoporous Materials under Loading" by Saad Alafnan & Yucel Akkutlu, 2017. Journal of Transport in Porous Media.

Taking the log of both sides, then the plot of the right hand side versus the left hand side in the Cartesian coordinate should be a straight line with y-intercept = 0. That is validated using the data obtained from the network as shown in Figure 28.

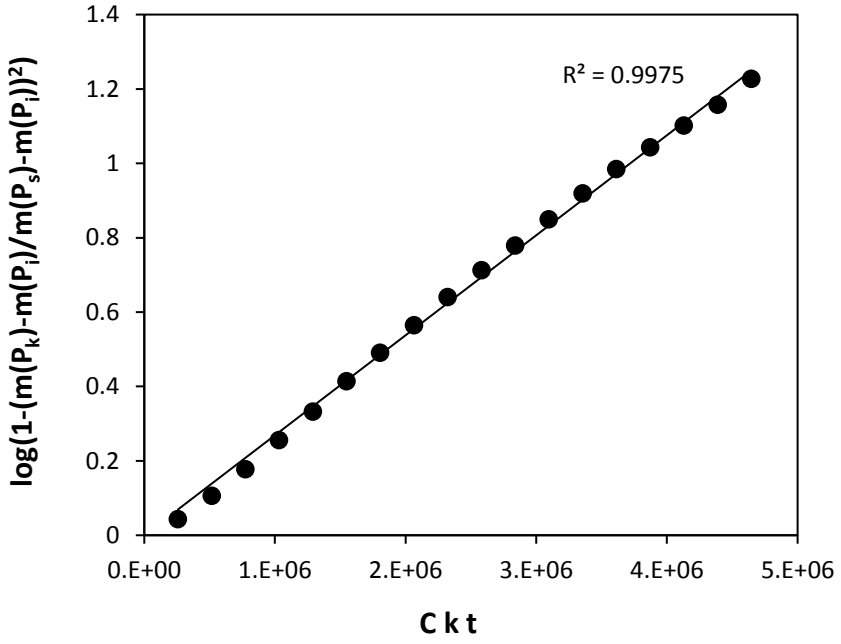

Figure 29 — Validation of the modified Crank sphere model using the results obtained from the network model.

APPENDIX C

DISCRETIZATION OF EQUATIONS 37 AND 38

For the field scale simulation, we are solving for the pressure at each gridblock using equations 37 and 38. The gas density is expressed is given in pressure using the real gas law. The following is an example of 1-D discretized forms at time t_i and gridblock m:

$$\frac{M}{\Delta t\ RT}\left[\left(P_{m,f}\ \emptyset\left(1-\varepsilon_{kp}\right)\right)_{t_i}-\left(P_{m,f}\ \emptyset\left(1-\varepsilon_{kp}\right)\right)_{t_{i+1}}\right] \tag{54}$$

$$=\frac{M\ k_f}{\Delta x^2 RT(\mu z)_{avg}}\left(P_{m,f}^2-P_{m-1,f}^2\right)+\frac{M\ k_f}{\Delta x^2 RT(\mu z)_{avg}}\left(P_{m+1,f}^2-P_{m,f}^2\right)-Q$$

$$\frac{M}{\Delta t\ RT}\left[\left(P_{m,om}\emptyset\left(\varepsilon_{kp}-\varepsilon_{ks}\right)\right)_{t_i}-\left(P_{m,om}\emptyset\left(\varepsilon_{kp}-\varepsilon_{ks}\right)\right)_{t_{i+1}}\right]=Q \tag{55}$$

$$Q=\sigma_{pss}k\ f_T[\psi\left(P_{m,om_{t_{i+1}}}\right)-\psi\left(P_{m,f_{t_{i+1}}}\right)] \tag{55}$$

Then, the above three equations are solved simultaneously using the iterative Newton Raphson method. All pressure dependent terms are updated at each time step.

$$\varepsilon_{ks}=\frac{V_s}{V},\qquad V_s=V_{sL}\frac{P}{P_L+P} \tag{56}$$

$$\emptyset_{om} = \emptyset_{om,i} \exp\left(-c_{om}(P_i - P)\right) \quad (57)$$

$$\emptyset_f = \emptyset_{f,i} \exp\left(-c_f(P_i - P)\right) \quad (58)$$

$$\varepsilon_k = \frac{\emptyset_{om}}{\emptyset_{om} + \emptyset_f} \quad (59)$$

where, V_s and P_L are the Langmuir isotherm parameters. $\emptyset_{om,i}$ and $\emptyset_{f,i}$ are the organic matter and crack porosities at the initial pressure P_i.